

---

# Shifts: A Dataset of Real Distributional Shift Across Multiple Large-Scale Tasks

---

Andrey Malinin<sup>1,2</sup>      Neil Band<sup>5</sup>      Alexander Ganshin<sup>1</sup>      German Chesnokov<sup>1</sup>  
 Yarin Gal<sup>5,6</sup>      Mark J. F. Gales<sup>4</sup>      Alexey Noskov<sup>1</sup>      Andrey Ploskonosov<sup>1</sup>  
 Liudmila Prokhorenkova<sup>1,2,3</sup>      Ivan Prosvirkov<sup>1</sup>      Vatsal Raina<sup>4</sup>      Vyas Raina<sup>4</sup>  
 Denis Roginskiy<sup>1</sup>      Mariya Shmatova<sup>1</sup>      Panos Tigas<sup>5</sup>      Boris Yangel<sup>1</sup>  
 am969@yandex-team.ru

## Abstract

There has been significant research done on developing methods for improving robustness to distributional shift and uncertainty estimation. In contrast, only limited work has examined developing standard datasets and benchmarks for assessing these approaches. Additionally, most work on uncertainty estimation and robustness has developed new techniques based on small-scale regression or image classification tasks. However, many tasks of practical interest have different modalities, such as tabular data, audio, text, or sensor data, which offer significant challenges involving regression and discrete or continuous structured prediction. Thus, given the current state of the field, a standardized large-scale dataset of tasks across a range of modalities affected by distributional shifts is necessary. This will enable researchers to meaningfully evaluate the plethora of recently developed uncertainty quantification methods, as well as assessment criteria and state-of-the-art baselines. In this work, we propose the *Shifts Dataset* for evaluation of uncertainty estimates and robustness to distributional shift. The dataset, which has been collected from industrial sources and services, is composed of three tasks, with each corresponding to a particular data modality: tabular weather prediction, machine translation, and self-driving car (SDC) vehicle motion prediction. All of these data modalities and tasks are affected by real, ‘in-the-wild’ distributional shifts and pose interesting challenges with respect to uncertainty estimation. In this work we provide a description of the dataset and baseline results for all tasks.

## 1 Introduction

Machine learning models are being applied to numerous areas [1, 2, 3, 4, 5, 6] and are being widely deployed in production. An assumption which pervades all of machine learning is that the training, validation, and test data are independent and identically distributed (i.i.d.). Thus, good performance and generalization on test data imply that the model will perform well in deployment. Unfortunately, this assumption seldom holds in real, “in the wild”, applications of machine learning. In practice, data are subject to a wide range of possible *distributional shifts* — mismatches between the training data, and test or deployment data [7, 8]. In general, the greater the degree of shift, the poorer is the model’s performance. The problems of uncertainty estimation and robustness to distributional shift are of relevance not only to academic researchers, but to the machine learning community at-large. Indeed, *all* ML practitioners have faced the issue of mismatch between the training and test sets. This

---

<sup>1</sup>Yandex, <sup>2</sup>HSE University, <sup>3</sup>Moscow Institute of Physics and Technology, <sup>4</sup>University of Cambridge, <sup>5</sup>University of Oxford, <sup>6</sup>Alan Turing Institute

is especially important in high-risk applications of machine learning, such as finance, medicine, and autonomous vehicles. Indeed, in such applications a mistake on part of an ML system may incur financial or reputational loss, or possible loss of life. It is therefore increasingly important to assess both a model’s *robustness* to distribution shift and its estimates of *predictive uncertainty*, which enable it to detect distributional shifts [9, 10, 11].

In the last few years the area of uncertainty estimation and robustness has developed rapidly. Model averaging [12, 13, 14, 15] has emerged as the de-facto standard approach to uncertainty estimation. Ensemble- and sampling-based uncertainty estimates have been successfully applied in detecting misclassifications, out-of-distribution inputs, adversarial attacks [16, 17], and active learning [18]. Recently, such approaches have been extended to structured prediction tasks such as machine translation and speech recognition [19, 20, 21, 22, 23]. However, ensemble- and sampling-based approaches require large computational and memory budgets. Works using temperature scaling [24, 25] and other recent approaches in deterministic uncertainty estimation [26, 27, 28, 29, 30] aim to tackle this issue, but have only recently begun to outperform the uncertainty estimates of ensemble methods [29, 30]. A range of methods called Prior Networks [31, 32, 33] — models which *emulate* the mechanics of an ensemble — have been proposed as a deterministic single model approach to uncertainty estimation, and are competitive with ensembles. However, they require distributionally shifted training data, which may not be feasible in many applications. Prior Networks have also been used for *Ensemble Distribution Distillation* [34, 33, 35] — a distillation approach through which the predictive performance and uncertainty estimates of an ensemble are captured within a single Prior Network, reducing the inference cost to that of a single model.

While much work has been done on developing *methods*, limited work has focused on new datasets and benchmarks. In [36], the authors introduced a benchmark for uncertainty quantification in Bayesian deep learning but only considered the image-based task of classifying diabetic retinopathy. Recently, a range of works by Hendrycks et al. [37, 38, 39] proposed a set of datasets based on ImageNet [40] for evaluating model robustness to various types of distributional shifts. These datasets — ImageNet C, A, R, and O — include synthetically added noise, natural adversarial attacks, renderings, and previously unseen classes of objects.<sup>1</sup> The release of WILDS, a collection of datasets containing real-world distributional shifts [8], similarly represents a significant step forward, but again mostly focuses on images. Finally, the MTNT dataset [41], which contains many examples of highly atypical usage of language, such as acronyms, profanity, emojis, slang, and code-switching, has been used at the Workshop on Machine Translation (WMT) robustness track. However, it has not been considered by the uncertainty community in the context of *detecting* distributional shift.

Unfortunately, with a few exceptions, most work on uncertainty estimation and robustness has focused on developing new methods on small-scale tabular regression or image classification tasks, such as UCI, MNIST [42], Omniglot [43], SVHN [44], and CIFAR10/100 [45]. Few works have been evaluated on the ImageNet variations A, R, C, and O, or WILDS. However, even evaluation on these datasets is limited, as they mainly focus on classification of images, and sometimes text. In contrast, many tasks of practical interest have different modalities, such as tabular data (in medicine and finance), audio, text, or sensor data. Furthermore, these tasks are not always classification; rather, they often involve regression and discrete or continuous structured prediction. Given the current state of the field, we aim to draw the attention of the community to the evaluation of uncertainty estimation and robustness to distributional shift on a realistic set of large-scale tasks across a range of modalities. This is necessary to meaningfully evaluate the plethora of methods for uncertainty quantification and improved robustness, accelerate the development of this area, and of safe ML in general.

In this work we propose the **Shifts Dataset**<sup>2</sup> for evaluation of uncertainty estimates and robustness to distributional shift. This dataset consists of data taken directly from large-scale industrial sources and services where distributional shift is ubiquitous. In this sense, the setting is as close to “in the wild” as possible. The dataset is composed of three parts, with each corresponding to a particular data modality: *tabular weather prediction* data provided by the Yandex.Weather service; *machine translation* data taken from the WMT robustness track and mined from Reddit, and annotated in-house by Yandex.Translate; and, *self-driving car (SDC)* data provided by Yandex SDG, for the task of *vehicle motion prediction*. All of these data modalities and tasks are affected by distributional shift

---

<sup>1</sup>ImageNet has only “natural” images; thus, renderings represent a texture shift while keeping the content unchanged.

<sup>2</sup>Data and example code are available at <https://github.com/yandex-research/shifts>

and pose interesting challenges with respect to uncertainty estimation. In this work we provide a detailed analysis of the data as well as baseline uncertainty estimation and robustness results using ensemble methods.

## 2 Assessment Metrics

Before we describe the Shifts Dataset, it is first necessary to discuss how to jointly assess uncertainty estimation and robustness to distributional shift. In most prior work on uncertainty estimation and robustness the two have been assessed separately. Robustness to distributional shift is typically assessed via metrics of predictive performance on a particular task, such as classification error-rate, BLEU, ADE, etc.. Here, given two (or more) evaluation sets, where one is considered matched to the training data and the other(s) is considered shifted, models which have a smaller degradation in performance on the shifted data are considered more robust. For example, the ImageNet C, R, and A variation datasets [39, 38, 37] were introduced specifically for the purpose of evaluating robustness to various forms of synthetic noise, significant shifts in texture and natural adversarial attacks. At the same time, the quality of uncertainty estimates is often assessed via the ability to discriminate between an 'in-domain' dataset which is matched to the training data and a shifted or 'out-of-domain' (OOD) dataset based on measures of uncertainty. Performance is typically assessed via Area under a Receiver-Operator Curve (ROC-AUC %) or Precision-Recall curve (AUPR %).

While these evaluation paradigms are meaningful, we believe that they are two halves of a common whole. In this work, we consider the following paradigm, which we believe is more general.

*As the degree of distributional shift increases, so does the likelihood that a model makes an error. For regression tasks, the degree of distributional shift is expected to correlate with the degree of error. Thus, models should yield a measure of uncertainty which correlates with the degree with distributional shift, and which therefore is indicative of the likelihood of an incorrect prediction or the degree of the error in the prediction.*

We believe that this paradigm is more general, as a model may be robust to certain examples of distributional shift, and therefore yield accurate predictions and low uncertainty of these examples. Similarly, a model may be aware that it is performing poorly on data which is matched to the training set and yield a high estimate of uncertainty. Such data could, for example, come from an underrepresented part of the training set. In this case, simply splitting the data into 'in-domain' and 'out-of-distribution' may not partition it into data on which it will perform well and data on which it will perform poorly. Thus, it is necessary to *jointly* assess robustness and uncertainty estimation, in order to see whether measures of uncertainty correlate well with the presence of an incorrect prediction or a high degree of error.

Our approach to jointly assess robustness and uncertainty are *error-retention curves* [11, 13], which depict the error over a dataset as a model's predictions are replaced by ground-truth labels in order of decreasing uncertainty. This represents a hybrid human-AI scenario, where a model can consult an oracle (human) for assistance in difficult situations. The area under this curve can be decreased either by making the model better, such that it has lower overall error, or by providing better estimates of uncertainty, such that more errorful predictions are rejected earlier. Thus, the area under the retention curve (R-AUC) is a metric for jointly assessing robustness to distributional shift and the quality of the uncertainty estimates. However, it is important that the dataset in question contains both a 'matched' subset and a distributionally shifted subset.

Figure 1 provides example retention curves for the three tasks of the Shifts Dataset. In addition to the uncertainty-based ranking, we included curves which represent 'random' ranking, where uncertainty estimates are entirely non-informative, and 'optimal' ranking, where uncertainty estimates perfectly correlate with error. These represent the lower and upper bounds on reducing area under the curve via uncertainty estimates.

While clearly interpretable and intuitive, one concern that can be raised regarding error-retention curves is that they can be more sensitive to predictive performance than to the quality of uncertainty estimates, which can be seen in Figure 1b, which occurs on tasks where most errors have similar magnitude. Furthermore, for regression tasks retention curves are dominated by noise in the targets

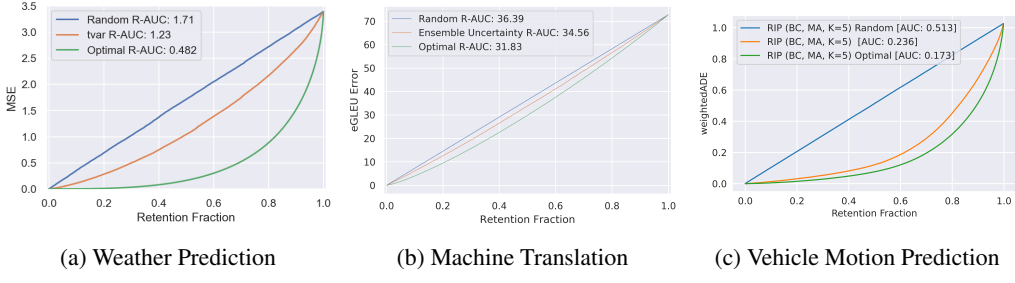


Figure 1: Example error retention curves for the three tasks of the Shifts Dataset.

(aleatoric uncertainty) at low retention, when most systematic errors have been detected already. Thus, in this work we propose another metric which jointly assesses robustness and uncertainty estimation.

First, we introduce the notion of ‘acceptable prediction’, which is a prediction whose error is acceptably small. This concept is natural to tasks with a non-binary notion of error, e.g., regression problems. For classification tasks, where predictions are already either correct or incorrect (acceptable/non-acceptable), this concept can be introduced by considering different levels of risk for different misclassifications. Formally, we say that a prediction is acceptable if an appropriate metric of error or risk is below a task-dependant threshold. This allows us to mitigate the issue of errors having similar magnitudes.

For a given dataset, we first determine which predictions are acceptable, given ground truth labels. Then, we use a model’s estimates of uncertainty to predict whether a prediction is acceptable or not. We calculate F1 for this binary classification task as for all detection thresholds and plot a curve of F1 vs. retention, as follows:

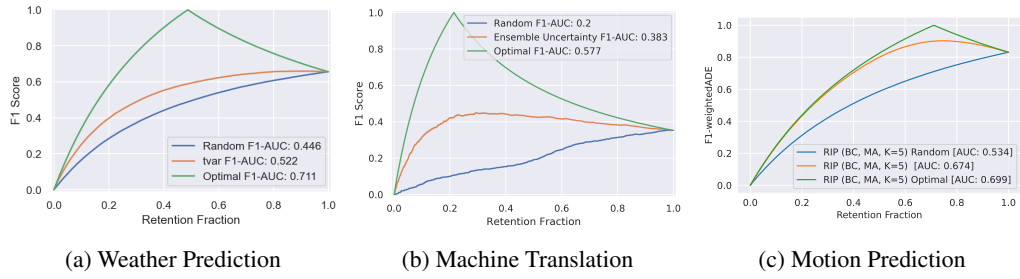


Figure 2: Examples of F1-Retention Curves for the three tasks of the Shifts Dataset

Here we plot both the uncertainty-based F1-retention curves for all models as well as the ‘random’ and ‘optimal’ baselines. Better models have higher area under F1-retention curve. The predictive performance of the model defines the starting point at 100% retention - better models start higher. Clearly, in contrast to Figure 1, the quality of the ranking affects area under the curve far more than for error-retention curves.

Area under the error-retention curve and F1-retention curve is a *summary statistic*, when describes the possible operating points. We can specify a particular operating points, such as 95% retention, and evaluate the error or F1 at that point for comparison. This is also an important figure, as all models work at a particular operating point which satisfies task-specific desiderata. In this work the desiderata for all tasks will be to not reject more than 95% of the input data.

### 3 Tabular Weather Prediction

Uncertainty estimation and robustness are essential in applications like medical diagnostics and financial forecasting. In such applications, data is often represented in a heterogeneous tabular form. While it is challenging to obtain either a large medical or financial dataset, the Yandex.Weather service has provided a large tabular weather prediction dataset which features a natural tendency

for the data distribution to drift over time. Furthermore, the locations are non-uniformly distributed around the globe based on population density, land coverage and observation network development, which means that certain climate zones, like the Polar regions or the Sahara, are under-represented. We argue that this tabular weather prediction data represents similar challenges to the ones faced on financial and medical data, which is often combined from different hospitals/labs, consists of population-groups which are non-uniformly represented and has a tendency to drift over time. Thus, the data which we consider in this paper can be used as an appropriate benchmark for developing more robust models and uncertainty estimation methods for tabular data.

In the Shifts weather prediction dataset, the goal is to predict the air temperature at 2 meters above ground at a particular latitude/longitude and timestamp, given all available weather station measurements and multiple weather forecast model predictions. In this regard, the task is a straightforward scalar regression task. However, except that a few features are removed due to privacy constraints, this is a real task and a dataset used by a commercial company for real-time weather forecasts <sup>3</sup> and is therefore entirely representative of an actual industrial application.

### 3.1 Dataset Description

The data consists of pairs of meteorological features and air temperature measurements at 2 metres above ground at a particular latitude/longitude and time. The feature vectors include both weather related features such as sun evaluation at the current location, climate values of temperature, pressure and topography, and meteorological parameters on different pressure and surface levels from *weather forecast model predictions*. *Weather forecast model predictions* are values produced by the following weather forecast models: Global Forecast System (GFS),<sup>4</sup> Global Deterministic Forecast System from the Canadian Meteorological Center (CMC),<sup>5</sup> and the Weather Research and Forecasting (WRF) Model.<sup>6</sup> Each model returns the following predicted values: wind, humidity, pressure, clouds, precipitation, dew point, snow depth, air and soil temperature characteristics. Where applicable, the predictions are given at different isobaric levels from 50 hPa ( $\approx$  20 km above ground) to the ground level. The GFS and WRF models run 4 time a day (0, 6, 12 and 18 GMT), and the CMC model runs twice a day (0 and 12 GMT). Model spatial grid resolution is  $0.25^\circ \times 0.25^\circ$  for GFS and  $0.24^\circ \times 0.24^\circ$  for CMC. The WRF model is calculated for over 60 domains all over the globe, spatial resolution for each domain is  $6 \times 6$  km. Altogether, there are 111 features in total. It is important to note that the features are highly heterogeneous, i.e., they are of different types and scales. The target air temperature values at different locations are taken from about 8K weather stations located across the globe, each of which periodically ( $\approx$  each 3 hours) reports a set of measurements. This dataset is provided under the CC BY NC SA 4.0 license.

To analyze the robustness of learned models to *climate shifts*, we use the Koppen climate classification [46] that provides publicly available data<sup>7</sup> that maps latitudes and longitudes at a  $0.5^\circ$  resolution to one of five main climate types: *Tropical*, *Dry*, *Mild Temperate*, *Snow* and *Polar*. This information is available over the years 1901 to 2010. The Weather Prediction dataset is augmented such that each sample has an associated climate type. The climate type is determined by minimizing the 1-norm between the longitudes/latitudes in the weather data and the Koppen climate classification for the most recent year available, 2010. The climate type is not used as a training feature.

There are 10M records in the full dataset distributed uniformly between September 1<sup>st</sup>, 2018, and September 1<sup>st</sup>, 2019, with samples across all five climate types. To test the robustness of the models, we evaluate how well they perform on time-shifted and climate-shifted data. Model performance is expected to decrease with time and climate shifts. However, a robust model is expected to be stable with these shifts.

---

<sup>3</sup><https://yandex.com/weather/meteum>

<sup>4</sup><https://www.ncdc.noaa.gov/data-access/model-data/model-datasets/global-forecast-system-gfs>

<sup>5</sup>[https://weather.gc.ca/grib/grib2\\_glb\\_25km\\_e.html](https://weather.gc.ca/grib/grib2_glb_25km_e.html)

<sup>6</sup><https://www.mmm.ucar.edu/weather-research-and-forecasting-model>

<sup>7</sup> Available to download from <http://hanschen.org/koppen>

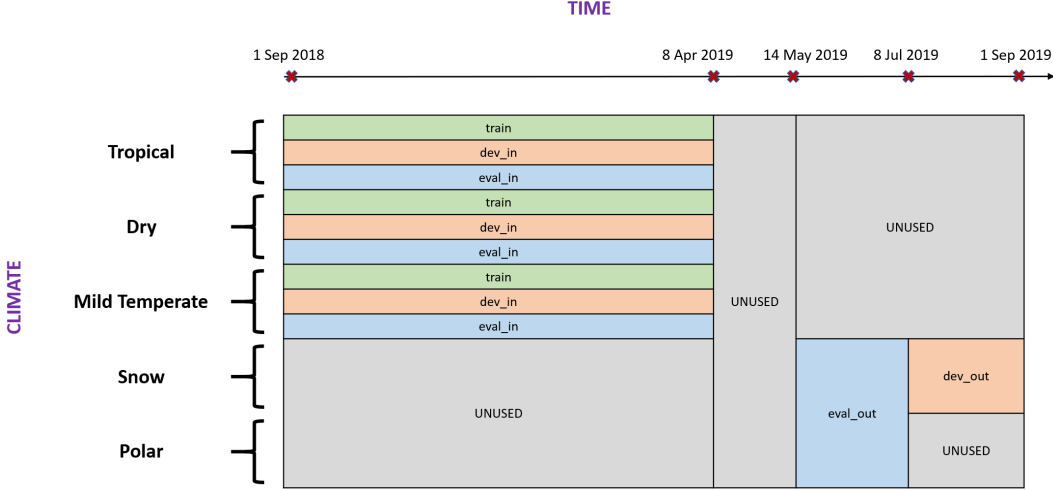


Figure 3: Canonical Partitioning of Weather Prediction dataset.

In order to provide a standard benchmark which contains data which is both matched and shifted relative to the training set, we split the full dataset into ‘canonically partitioned’<sup>8</sup> training, development, and evaluation datasets as follows (see Figure 3):

- The training data consists of measurements made from September 2018 till April 8<sup>th</sup>, 2019 for climate types *Tropical*, *Dry*, and *Mild Temperate*.
- The development data is composed of in-domain (*dev\_in*) and out-of-domain (*dev\_out*) data. The in-domain data corresponds to the same time range and climate types as the training data. The out-of-domain development data consists of measurements made from 8<sup>th</sup> July till 1<sup>st</sup> September 2019 for the climate type *Snow*. 50K data points are subsampled for the climate type *Snow* within this time range to construct *dev\_out*.
- The evaluation data is also composed of in-domain (*eval\_in*) and out-of-domain (*eval\_out*) data. As before, the in-domain data corresponds to the same time range and climate types as the training data. The out-of-domain evaluation data is further shifted than the out-of-domain development data; measurements are taken from 14<sup>th</sup> May till 8<sup>th</sup> July 2019, which is more distant in terms of the time of the year from the in-domain data compared to the out-of-domain development data. The climate types are restricted to *Snow* and *Polar*.

Table 1 details the number of samples in the selected partition of the data. It also details the number of samples for each climate type for each part of the dataset. The in-domain data is split in approximately 83.7-1.3-15% ratio between training, development, and evaluation. Figure 4 depicts the shift in the target temperatures between the training, development, and evaluation datasets. It is clear that the temperature distribution is different for *dev\_out* and *eval\_out* compared to the in-domain sets. The higher average temperature in the out of domain sets is perhaps due to the out of domain data being sourced from the Summer regions (for the northern hemisphere) while the in-domain data is largely sourced from the Winter time period. Figure 5 further shows the shift in the samples’ locations (latitudes/longitudes) between training, development, and evaluation datasets. The location shift is a natural result of the climate shifts present in the datasets where the training data tends to correspond to warmer parts of the world, whereas the development and evaluation datasets include colder climates too.

### 3.2 Metrics

We aim at comparing different models in terms of uncertainty estimation and robustness to distributional shifts. Several performance metrics are considered.

<sup>8</sup> Alternative partitioning can be made from the full data, but we will use the canonical partition throughout this work.

Table 1: Number of samples in the canonical partitioning of Weather Prediction dataset.

Data	Total	# of samples					
		Tropical	Dry	Mild	Temperate		
Training	train	<b>3,129,592</b>	416,310	690,284	2,022,998	0	0
Development	dev_in	<b>50,000</b>	6,641	10,961	32,398	0	0
	dev_out	<b>50,000</b>	0	0	0	50,000	0
	dev	<b>100,000</b>	6,641	10,961	32,398	50,000	0
Evaluation	eval_in	<b>561,105</b>	74,406	123,487	363,212	0	0
	eval_out	<b>576,626</b>	0	0	0	525,967	50,659
	eval	<b>1,137,731</b>	74,406	123,487	363,212	525,967	50,659

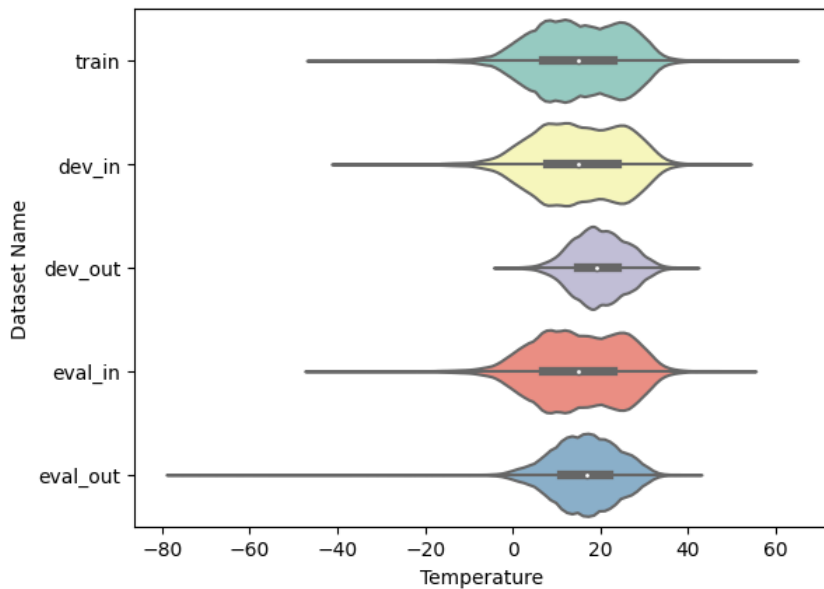


Figure 4: Temperature distributions on canonical partitions of Weather Prediction dataset.

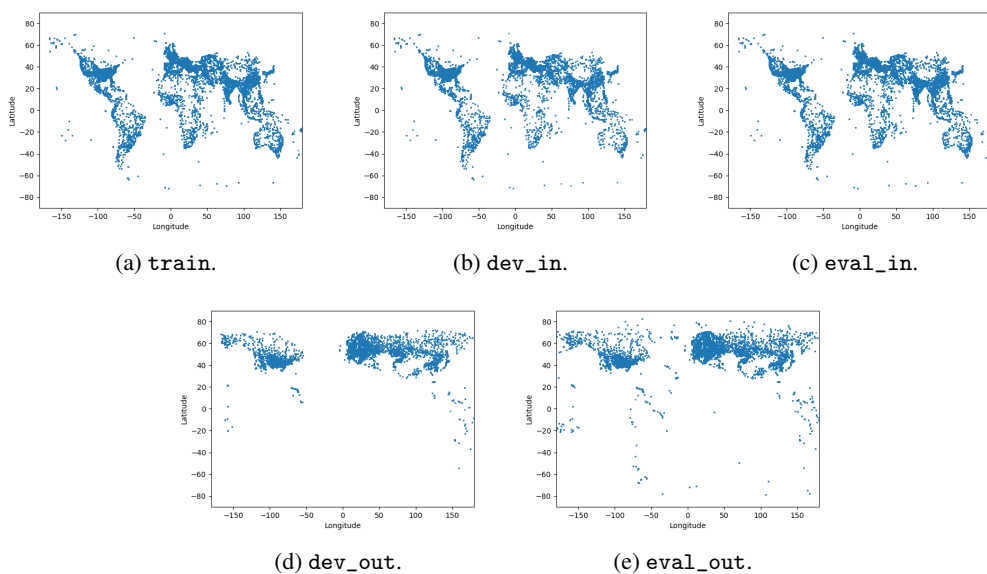


Figure 5: Location of samples from canonical partitioning of Weather Prediction dataset.

**Predictive Performance** Predictive performance and robustness to distributional shifts is evaluated by measuring RMSE and MAE between predictions and targets: lower the RMSE/MAE score on the test sets, greater the robustness of the models to the distributional shift.

**Joint assessment of Uncertainty and Robustness** We will jointly assess robustness and uncertainty estimation via error-retention and F1-retention curves, described in section 2. We will use MSE as the error metric instead of RMSE as it is linear with respect to the error for each datapoint. For the F1-retention curve an acceptable prediction is defined as one where  $\text{MSE} < 1.0$ . This corresponds to an error of 1 degree or less, which most people cannot feel. Typically people are sensitive to differences in surrounding temperature of over a degree. These two performance metrics are respectively denoted as R-AUC and F1-AUC. A good uncertainty measure is able to achieve low R-AUC and high F1-AUC. Additionally, the F1 score at a retention rate of 95% of the most certain samples is also quoted and is denoted as F1@95%, which is a single point summary jointly of the uncertainty and robustness. Finally, ROC-AUC is used as a summary statistic for evaluating uncertainty-based out-of-distribution data detection.

### 3.3 Baseline Results

To build baseline models for the temperature prediction regression task, we use the open-source CatBoost gradient boosting library that is known to achieve state-of-the-art results on various tabular datasets [47]. Here we consider an ensemble-based approach to uncertainty estimation for GBDT models [48]. An ensemble of ten models is trained on the `train` data from the canonical partition of the Weather Prediction dataset with different random seeds is used as the baseline. The models are optimized with the loss function `RMSEWithUncertainty` [48] that predicts mean and variance of the normal distribution by optimizing the negative log-likelihood. Each model is constructed with a depth of 8 and then is trained for 20,000 iterations at a learning rate of 0.3. Hyperparameter tuning is performed on the `dev_in` data.

As the uncertainty measure, we use the total variance (tvar) that is the sum of the variance of the predicted mean and the mean of the predicted variance as our chosen measure of uncertainty [48, 11, 10]. We also compare the ensemble with an individual model, where we use the predicted variance as an uncertainty measure.

Table 2: Predictive performance on the test sets from the canonical partitioning of Weather Prediction dataset. One standard deviation is quoted for the single seed results.

Data	RMSE		MAE	
	Single	Ens	Single	Ens
<code>dev</code>	$1.978 \pm 0.007$	1.842	$1.466 \pm 0.005$	1.361
<code>eval</code>	$2.164 \pm 0.006$	1.997	$1.555 \pm 0.006$	1.437

The predictive performance results are presented in Table 2. First, we measure RMSE of a single model and observe that it is about two degrees Celsius. As expected, the error is larger on the evaluation set. Ensembling allows us to reduce RMSE by about  $0.15^\circ$ . Similarly, ensembling reduces the MAE by approximately  $0.11^\circ$ .

Table 3: Retention performance on the test sets from the canonical partitioning of Weather Prediction dataset. One standard deviation is quoted for the single seed results.

Data	R-AUC		F1-AUC		F1@95%	
	Single	Ens	Single	Ens	Single	Ens
<code>dev</code>	$1.894 \pm 0.017$	1.227	$0.4435 \pm 0.002$	0.5220	$0.6272 \pm 0.001$	0.6583
<code>eval</code>	$2.320 \pm 0.063$	1.335	$0.4341 \pm 0.001$	0.5236	$0.6189 \pm 0.001$	0.6472

Then, in Table 3, we compute R-AUC, F1-AUC, and F1@95%. Here, as expected, ensembles significantly outperform single models. The associated retention curves are provided in Figure 6.

Table 4 presents a comparison of which measures of uncertainty are best for different tasks. We evaluate OOD detection via ROC-AUC as well as the F1-AUC performance metric values for different

Table 4: Comparing ensembled F1-AUC and ROC-AUC for various uncertainty measures on the tests sets from the canonical partitioning of Weather Prediction dataset.

Data		Uncertainty measure				
		mvar	varm	tvar	epkl	random
dev	F1-AUC	0.4951	0.5012	<b>0.5220</b>	0.5051	0.4446
	ROC-AUC	0.4755	0.8231	0.6296	<b>0.8529</b>	0.5000
eval	F1-AUC	0.4873	0.4981	<b>0.5236</b>	0.5040	0.4393
	ROC-AUC	0.4956	0.7832	0.6599	<b>0.7990</b>	0.5000

uncertainty measures. We consider mean across ensemble of the predicted variances (mvar), a measure of *data uncertainty*; variance across ensemble of the mean predictions (varm) and expected pairwise KL-divergence (epkl), which are measures of *knowledge uncertainty*, and total variance, which is the sum of varm and mvar, a measure of *total uncertainty*. The results show that uncertainty measures that capture knowledge uncertainty, such as varm and epkl, perform best at out of distribution detection, as suggested by the high ROC-AUC values, whilst the measures of total uncertainty perform best for detecting errors. Measures of data uncertainty perform worse than others on both tasks. This shows that the choice of metric to use depends heavily on the task. Similarly, any conclusions about "which metric is best" depend on the evaluation methodology.

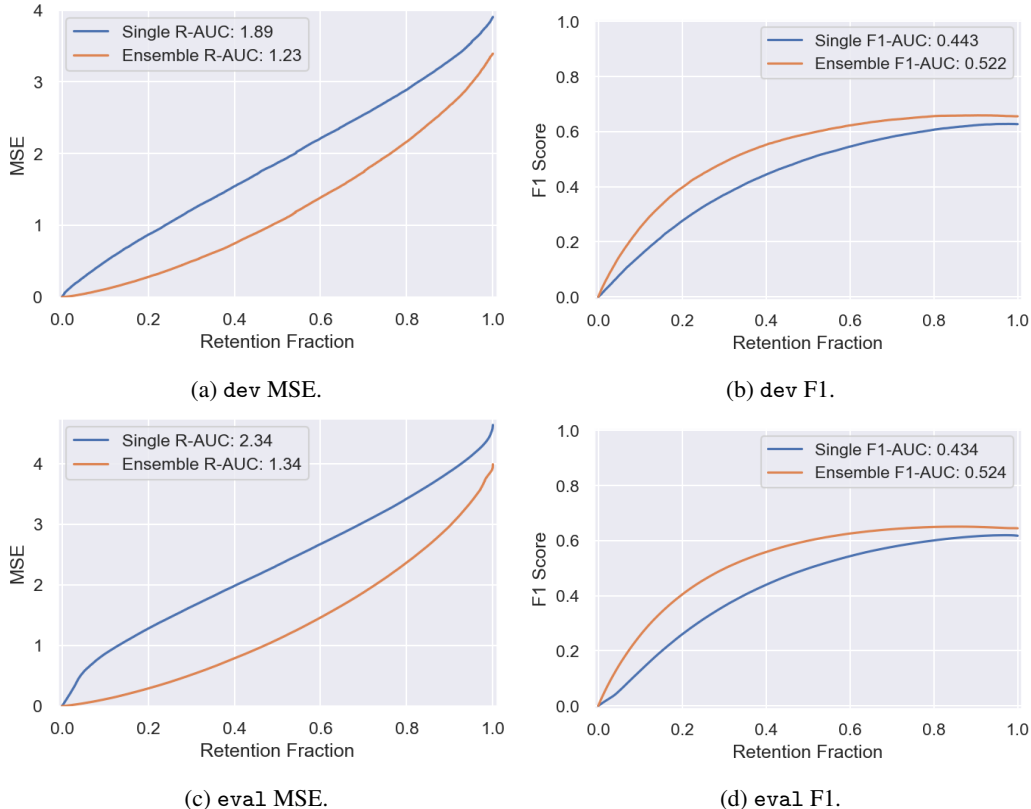


Figure 6: MSE/F1 retention curves on dev and eval from the canonical partitioning of Weather Prediction dataset.

## 4 Machine Translation

As part of the Shifts dataset we examine the task of machine translation for the text modality. Translation services, such as Google Translate or Yandex Translate, often encounter atypical and unusual use of language in their translation queries. This typically includes slang, profanities,

poor grammar, orthography and punctuation, as well as emojis. This poses a challenge to modern translation systems, which are typically trained on corpora with a more “standard” use of language. Therefore, it is important for models to be robust to atypical language use and provide high-quality translations under such a distribution shift as well as indicate when they are unable to provide a quality translation.

As there are dependencies between the tokens in the output sequence of a translation model, translation is inherently a *structured prediction* task. Often we must make assumptions about the form of these dependencies; for example, most modern translation systems are left-to-right autoregressive. However, we could consider conditionally independent predictions or other factorization orders. The nature of these assumptions makes it challenging to obtain a theoretically sound measure of uncertainty. Only recently has work been done on developing principled uncertainty measures for structured prediction tasks [23, 22, 49, 21, 20]. This makes the area particularly appealing for uncertainty and robustness research.

#### 4.1 Dataset Description

As most production NMT systems are built using a variety of general purpose corpora, we do not provide a new training corpus – only development and evaluation data. We will use the freely available WMT’20 English-Russian corpus, which covers a variety of domains, but primarily focuses on parliamentary and news data. For the most part, this data is grammatically and orthographically correct and language use is formal. This is representative of the type of data used, for example, to build the Yandex.Translate NMT system. As part of the Shifts dataset we provide two “in-domain” or non-distributionally shifted datasets. We select the English-Russian Newstest’19 as the *development set* and will use a corpus of news data collected from GlobalVoices News service [50] and manually annotated using expert human translators as heldout *evaluation set*.

For the shifted development and evaluation data we will consider the Reddit corpus prepared for the WMT’19 robustness challenge [41]. This data contains examples of slang, acronyms, lack of punctuation, poor orthography, concatenations, profanity, and poor grammar, among other forms of atypical language usage. This data is representative of the types of inputs that machine translation services find challenging. As Russian target annotations are not available, we pass the data through a two-stage process, where orthographic, grammatical and punctuation mistakes are corrected, and the source-side English sentences are translated into Russian by expert translators. The development set is constructed from the 1400-sentence test-set used for the WMT’19 robustness challenge. For the heldout evaluation set we use the open-source MTNT crawler to collect a further set of 3,000 English sentences from Reddit, which will be similarly corrected and translated. In terms of size, these development and test sets are comparable or larger to the ones used in the WMT challenges and for evaluating production systems.

**License** The source-side sentences, crawled from Reddit are released under the terms of the Reddit API. The target-side translations, produced in-house at Yandex, are released under CC BY NC SA 4.0 .

Table 5: NMT Data Description - All Data is English-Russian

Data Set	N. Sentences	Type
WMT’20	70M	Train
NWT’19	1997	In-domain Dev
GlobalVoices	3,000	In-domain Eval
WMT’19 MTNT Reddit	1,362	Shifted Dev
Shifts Reddit	3,065	Shifted Eval

Both the development and evaluation Reddit data is annotated with the follow 7 non-exclusive anomaly flags:

- **Punctuation anomalies:** Some punctuation marks are missed or used incorrectly or some formatting (like Wiki markup) is used in the sentence.

- **Spelling anomalies:** The sentence contains spelling errors, including incorrect concatenation of two words as well as incorrect use of hyphens.
- **Capitalization anomalies:** Words that should be capitalized according to the language rules are written in lower case or vice versa.
- **Fluency anomalies:** The sentence is non-fluent due to wrong or missing prepositions, pronouns or ungrammatical form choice.
- **Slang anomalies:** In the sentence there are slang words or abbreviations like “idk” for “I don’t know” or “cuz” for “because”.
- **Emoji anomalies:** The sentence contains emojis either at the end of it, or instead of some words.
- **Tags anomalies:** The sentence contains markup for usernames or code like “r/username”.

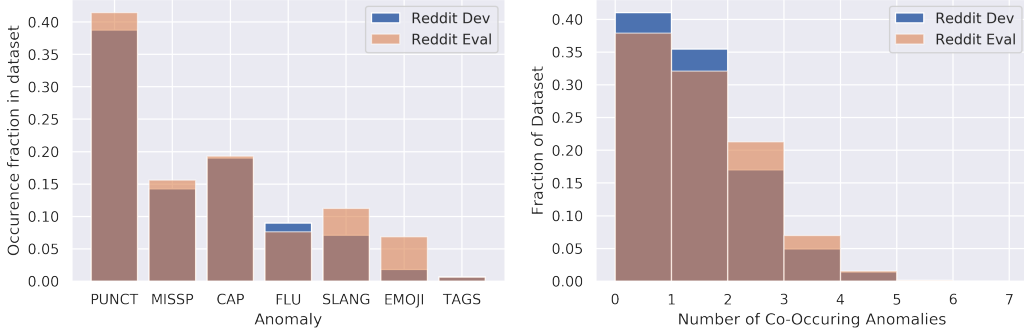


Figure 7: Analysis of anomaly occurrence and co-occurrence in Reddit (shifted) development and evaluation data

## 4.2 Metrics

To evaluate the performance of our models we will consider the following two metrics : corpus-level BLEU [51] and sentence-level GLEU [52, 53, 54]. GLEU is an analogue of BLEU which is stable when computed at the level of individual sentences. Thus, it is far more useful at evaluating system performance on a per-sample basis, rather than at the level of an entire corpus. Note that GLEU correlates strongly with BLEU at the corpus level.

Machine translation is inherently a multi-modal task, as a sentence can be translated in multiple equally valid ways. Furthermore, translation systems often yield multiple translation hypothesis. To account for this we will consider two GLEU-based metrics for evaluating translation quality. First is the *expected GLEU* or **eGLEU** across all translation hypotheses returned by a translation models. Each hypothesis is assumed to be assigned a *confidence score*, and confidences across each hypotheses by sum to one. This is our primary assessment metric:

$$\text{eGLEU} = \frac{1}{N} \sum_{i=1}^N \sum_{h=1}^H \text{GLEU}_{i,h} \cdot w_{i,h}, \quad w_{i,h} > 0, \sum_{h=1}^H w_h = 1 \quad (1)$$

Additionally, we will consider the *maximum GLEU* or **maxGLEU** across all hypothesis, which represents an upper bound on performance, given a model can appropriately rank it’s hypotheses:

$$\text{maxGLEU} = \frac{1}{N} \sum_{i=1}^N \max_h [\text{GLEU}_{i,h}] \quad (2)$$

Finally, in order to calculate area under the error retention curve we need to introduce an *error metric*, where lower error is better. This is trivially done by introducing *eGLEU error*, which defined as:

$$\text{eGLEU Error} = 100 - \text{eGLEU} \quad (3)$$

Thus, in the next section, area under the error retention curve (R-AUC), as well as the F1 metric for detecting ‘valid predictions’ will be calculated using eGLEU Error.

### 4.3 Baseline Results

In this work we considered a simple ensemble baseline based on [23]. Here, we consider an ensemble of 3 Transformer-Big [5] models trained on the WMT’20 En-Ru corpus. Models were trained using a fork of FairSeq [55] using a large-batch training set. Beam-Search decoding with a beam-width of 5 is used to obtain translation hypotheses. Hypotheses confidence weights are obtained by exponentiating the negative log-likelihood of each hypothesis and then normalizing across all hypotheses in the beam. In addition, we also consider a single-model baseline by using the models in the ensemble individually.

The results in table 6 show the BLEU, eGLEU and maxGLEU for the in-domain development set (dev-in), Newstest’19, the shifted development set based on MTNT [41] (dev-out) and the joint development set. Clearly, there is a performance difference of nearly 10 BLEU and GLEU points between the in-domain and shifted data. This clearly shows the degradation in quality due to the presence of a-typical language usage. The ensemble is able to outperform the individual models, which is expected. Additionally, these results show that BLEU correlates quite well with eGLEU. maxGLEU shows that significantly better performance is obtainable if we were able to always choose the best one from the beam.

Table 6: Predictive Performance. One standard deviation is quoted for the single seed results.

Data	BLEU		eGLEU		maxGLEU	
	Single	Ens	Single	Ens	Single	Ens
dev-in	32.04 $\pm$ 0.23	32.73	34.45 $\pm$ 0.10	35.09	41.08 $\pm$ 0.09	42.00
dev-out	20.65 $\pm$ 0.16	21.06	22.66 $\pm$ 0.07	23.00	28.28 $\pm$ 0.19	28.63
dev	28.89 $\pm$ 0.20	29.52	29.67 $\pm$ 0.09	30.19	35.89 $\pm$ 0.12	36.58
eval-in	29.52 $\pm$ 0.21	30.08	30.39 $\pm$ 0.10	30.88	36.19 $\pm$ 0.19	36.82
eval-out	21.00 $\pm$ 0.12	21.54	23.19 $\pm$ 0.07	23.60	29.35 $\pm$ 0.11	29.88
eval	26.39 $\pm$ 0.17	26.92	26.76 $\pm$ 0.06	27.20	32.74 $\pm$ 0.14	33.31

Having evaluating the baselines’ predictive performance, we now jointly assess their uncertainty and robustness using the area under the error-retention curve (R-AUC), area under the F1-retention curve (F1-AUC) and F1 at 95% retention. Additionally, we evaluate in terms of % ROC-AUC whether it is possible to discriminate between the in-domain data and the shifted data based on the measures of uncertainty provided by the models. As the measure of uncertainty we use the negative log-likelihood, averaged across all 5 hypotheses. In the case of individual models, this is a measure of *data* or *aleatoric* uncertainty, and in the case of the ensemble, it is a measure of *total uncertainty* [23]. The results show that the ensemble consistently outperforms the single-model baseline.

Table 7: Evaluation of Uncertainty Estimation and Robustness. One standard deviation is quoted for the single seed results.

Data	R-AUC		F1-AUC		F1@95%		ROC-AUC	
	Single	Ens	Single	Ens	Single	Ens	Single	Ens
dev	33.22 $\pm$ 0.48	32.87	0.428 $\pm$ 0.003	0.443	0.415 $\pm$ 0.006	0.432	68.9 $\pm$ 0.28	69.3
eval	34.8 $\pm$ 0.06	34.57	0.37 $\pm$ 0.07	0.38	0.34 $\pm$ 0.03	0.36	79.18 $\pm$ 0.63	80.1

## 5 Vehicle Motion Prediction

We present the Shifts Vehicle Motion Prediction dataset to examine the implications of distributional shift in self-driving vehicles. The area of autonomous vehicle (AV) technology is highly relevant for uncertainty and robustness research, as the safety requirements and the risks associated with any errors are high. Furthermore, distributional shift is ubiquitous in the autonomous driving domain. Most self-driving companies concentrate their fleet in a limited number of locations and routes due to the large cost of operating in an incremental location. Therefore, fleets often face distributional shift when they begin operation at a new location, or even a new route in an existing location. It is thus important to transfer as much knowledge as possible from the old locations to the new one.

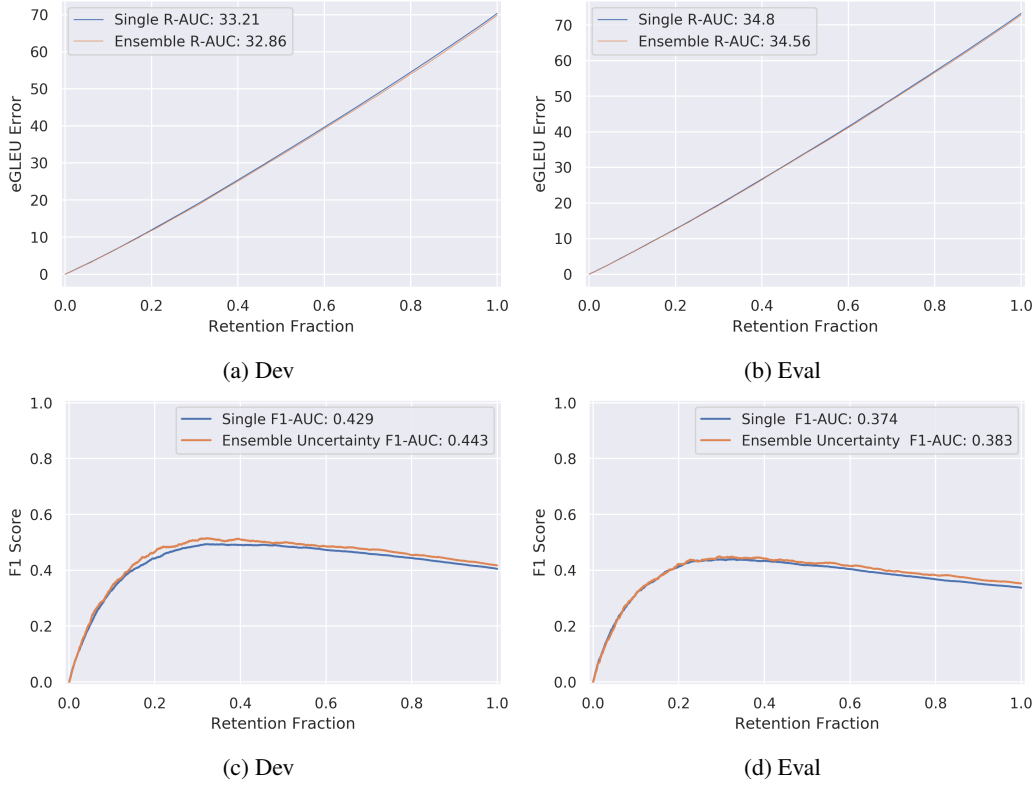


Figure 8: Location of samples from canonical partitioning of Weather Prediction dataset.

It is also critical for a planning model to recognize when this transferred knowledge is insufficient upon encountering unfamiliar data, which could risk unpredictable and unsafe behavior. Uncertainty quantification therefore has potentially life-critical application in this domain. For example, when the model’s predictive uncertainty reaches a particular threshold, the vehicle can exercise extra caution or even transfer control to the human driver [56].

The problem of motion prediction is among the most important in the autonomous driving domain and has recently drawn significant attention from both academia and industry [57, 58, 59, 60, 61, 62, 63, 64, 65, 66, 67, 68]. It involves predicting the distribution over possible future states of agents around the self-driving car at a number of moments in time. A model of possible futures is needed because a self-driving vehicle needs a certain amount of time to change its speed, and sudden changes may be uncomfortable or even dangerous for its passengers. Therefore, in order to ensure a safe and comfortable ride, a self-driving vehicle’s motion planning module needs to reason about where other agents might end up in a few seconds so that it doesn’t plan a potential collision.

This problem is additionally complicated by the fact that *the future is inherently uncertain*. For example, we cannot know the high-level navigational goals of other agents, or even their low-level tendency to turn right or left at a T-junction if they fail to indicate one way or another. In order for the planning module to make the right decision, this uncertainty must be precisely quantified.

Motion prediction is interesting not only due to its real-world application and the safety-critical nature of autonomous vehicle technology, but also because the predictions are both *structured and continuous*. This poses further challenges in uncertainty estimation. Recently, ensemble-based uncertainty estimation for the related task of autonomous vehicle *planning* was examined [69], where a variance-based measure was proposed. However, there is still much potential for further development of informative measures of uncertainty in continuous structured prediction tasks, such as motion prediction.

Table 8: A comparison of various motion prediction datasets. The Shifts Vehicle Motion Prediction dataset is the largest by number of scenes and total size in hours.

Dataset	Scene Length (s)	# Scenes			Total Size (h)	Avg. # Actors
		Train	Dev	Eval		
Argoverse	5	205,942	39,472	78,143	320	50
Lyft	25	134,000	11,000	16,000	1,118	79
Waymo	20	72,347	15,503	15,503	574	-
Shifts	10	500,000	50,000	50,000	1,667	29

### 5.1 Dataset Description

The dataset for the Vehicle Motion Prediction task was collected by the Yandex Self-Driving Group (SDG) fleet. This is the largest vehicle motion prediction dataset released to date, containing 600,000 scenes (see Table 8 for a comparison to other public datasets). We release this dataset under the CC BY NC SA 4.0 license. The dataset consists of scenes spanning six locations, three seasons, three times of day, and four weather conditions (cf. Table 9 and 10). Each of these conditions is available in the form of tags associated with every scene. Each scene is 10 seconds long and is divided into 5 seconds of context features and 5 seconds of ground truth targets for prediction, separated by the time  $T = 0$ . The goal of the task is to predict the movement trajectory of vehicles at time  $T \in (0, 5]$  based on the information available for time  $T \in [-5, 0]$ .

Table 9: The number of scenes in the Vehicle Motion Prediction dataset by location and season.

Location	Train	Dev	Eval	Season			
				Train	Dev	Eval	
Moscow	450,504	30,505	30,534	85,698	10,634	10,481	
Skolkovo	6,283	2,218	2,956	126,845	15,290	15,840	
Innopolis	15,086	5,164	5,016	287,457	24,076	23,679	
Ann Arbor	19,349	8,290	6,617	0	0	0	Spring
Modiin	3,502	2,262	1,555				
Tel Aviv	5,276	1,561	3,322				

Each scene includes information about the state of dynamic objects (i.e., vehicles, pedestrians) and an HD map. Each vehicle is described by its position, velocity, linear acceleration, and orientation (yaw, known up to  $\pm\pi$ ). A pedestrian state consists of a position vector and a velocity vector. All state components are represented in a common coordinate frame and sampled at 5Hz frequency by the perception stack running on the Yandex SDG fleet. The HD map includes lane information (e.g., traffic direction, lane priority, speed limit, traffic light association), road boundaries, crosswalks, and traffic light states, which are also sampled at 5Hz.<sup>9</sup>

The ground truth part of a scene contains future states of dynamic objects sampled at 5Hz for a total of 25 state samples. Some objects might not have all 25 states available due to occlusions or imperfections of the on-board perception system.

A number of vehicles in the scene are labeled as *prediction requests*. These are the vehicles that are visible at the most recent time  $T = 0$  in the context features part of a scene, and therefore would call for a prediction in a deployed system. For such vehicles we provide not only their future trajectories, but also a number of non-mutually exclusive tags (detailed in Table 11) describing the associated

<sup>9</sup>To facilitate easy use of this dataset, we provide utilities to render scene information as a feature map, which can be used as an input to a standard vision model (e.g., a ResNet [70]). Our utilities represent each scene as a birds-eye-view image with each channel corresponding to a particular feature (e.g., a vehicle occupancy map) at a particular timestep. We also provide pre-rendered feature maps for every prediction request (cf. Section 5.2) in the dataset, which are used to train the baseline models. The maps are  $128 \times 128$  pixels in size with each pixel covering 1 square meter, have 17 channels describing both HD map information and dynamic object states at time  $T = 0$ , and are centered with respect to the agent for which a prediction is being made. Researchers working with the dataset are free to use these feature maps, use the provided utilities to render another set of feature maps at different (earlier) timesteps, or construct their own scene representations from the raw data.

Table 10: The number of scenes in the Vehicle Motion Prediction dataset by precipitation and time of day.

Precipitation Type	Train	Dev	Eval	Sun Phase	Train	Dev	Eval
No	432,598	44,799	44,274	Astronomical Night	171,867	13,164	13,113
Rain	15,618	1,857	1,751	Daylight	299,065	33,879	33,979
Sleet	15,210	1,082	990	Twilight	29,068	2,957	2,908
Snow	36,574	2,262	2,985				

maneuver in more detail – whether the vehicle is turning, accelerating, slowing down, etc. – for a total of 10 maneuver types. Note that some prediction requests may not have all 25 state samples available. We call prediction requests with fully-observed state *valid* prediction requests and propose to evaluate predictions only on those.

Table 11: Number of actor maneuvers of the respective type.

Maneuver Type	Train	Dev	Eval
Move Left	254,843	25,049	25,820
Move Right	322,231	30,074	30,633
Move Forward	5,032,724	395,467	413,920
Move Back	54,677	4,811	4,891
Acceleration	2,473,750	206,977	215,009
Deceleration	2,050,186	168,550	174,477
Uniform Movement	6,369,920	566,083	573,033
Stopping	441,619	38,411	39,336
Starting	739,143	64,986	65,759
Stationary	4,620,678	433,161	433,576

In order to study the effects of distributional shift, as well as assess the robustness and uncertainty estimation of baseline models, we divide the Vehicle Motion Prediction dataset such that there are *in-domain* partitions which match the location and precipitation type of the training set, and *out-of-domain* or *shifted* partitions which do not match the training data along one or more of those axes. Furthermore, we provide a *development* set which acts as a validation set, and an *evaluation* set which acts as the test set. For benchmarking and reporting baseline performance results, we define a *canonical partitioning* of the full dataset (cf. Fig. 9, Table 12) as the following. The training, in-domain development, and in-domain evaluation data are taken from Moscow. Distributionally shifted development data is taken from Skolkovo, Modiin, and Innopolis. Distributionally shifted evaluation data is taken from Tel Aviv and Ann Arbor. In addition, we remove all cases of precipitation from the in-domain training, development, and test sets, while distributionally shifted datasets include precipitation. The canonical partitioning is fully described in Fig. 9. This partitioning will also be the one used in the Shifts Challenge.

	Moscow	Skolkovo	Modiin	Innopolis	Ann-Arbor	Tel Aviv
No precipitation	train					
	development in	development out	development out	development out	evaluation out	evaluation out
	evaluation in					
Rain	UNUSED	development out	development out	development out	evaluation out	evaluation out
Sleet	UNUSED	UNUSED	UNUSED	UNUSED	evaluation out	evaluation out
Snow	UNUSED	development out	development out	development out	evaluation out	evaluation out

Figure 9: The canonical partitioning of the Vehicle Motion Prediction dataset.

Table 12: The number of scenes in the canonical dataset partitioning.

Dataset Partition	In-Distribution	Distributionally Shifted
Train	388,406	-
Development	27,036	9,569
Evaluation	26,865	9,939

## 5.2 Task Setup

Vehicle Motion Prediction is a complex task and therefore must be described in detail. We provide a training dataset  $\mathcal{D}_{\text{train}} = \{(\mathbf{x}_i, \mathbf{y}_i)\}_{i=1}^N$  of time-profiled ground truth trajectories (i.e., plans)  $\mathbf{y}$  paired with high-dimensional observations (features)  $\mathbf{x}$  of the corresponding scenes. Each  $\mathbf{y} = (s_1, \dots, s_T)$  corresponds to the trajectory of a given vehicle observed through the SDG perception stack. Each state  $s_t$  corresponds to the x- and y-displacement of the vehicle at timestep  $t$ , s.t.  $\mathbf{y} \in \mathbb{R}^{T \times 2}$ . We consider the performance of models on development and evaluation datasets  $\mathcal{D}_{\text{dev}}^j = \{(\mathbf{x}_i, \mathbf{y}_i)\}_{i=1}^{M_j}$  and  $\mathcal{D}_{\text{eval}}^j = \{(\mathbf{x}_i, \mathbf{y}_i)\}_{i=1}^{M_j}$ . See Fig. 10 for a depiction of the task.

**Prediction Requests.** There are  $N$  ( $M_j$ ) prediction requests in the training dataset (evaluation datasets), with many requests for each scene corresponding to the many different vehicle trajectories observed. For example, in the canonical partition of the data, there are 388,406 scenes in the training dataset (Moscow, no precipitation), and 5,649,675 valid prediction requests.

Models can be trained to make use of ground truth trajectories that contain occlusions (i.e., prediction requests that are not valid) during training, such as through linear interpolation of missing steps. However, for the benchmarks considered in this work, both training and evaluation are done using only the fully observed ground truth trajectories.

Next, we describe the two levels of uncertainty quantification that we consider for each prediction request in the proposed task: per-trajectory and per-prediction request uncertainty scores.

**Per-Trajectory Confidence Scores.** Like machine translation, motion prediction is an inherently multimodal task. A motion prediction model can produce a different number of sampled trajectories (plans)  $D_i$  for each input  $\mathbf{x}_i$ ; in other words, for two inputs  $\mathbf{x}_i, \mathbf{x}_j$  with  $i \neq j$ ,  $D_i$  and  $D_j$  can differ. As a justification, consider that in a certain context, multiple trajectories may be desirable to capture multimodality (e.g., the vehicle of interest is at a T-junction), and in others a single or fewer trajectories would be sufficient (e.g., the vehicle is clearly proceeding straight). In our task, we expect a stochastic model to accompany its  $D_i$  predicted trajectories on a given input  $\mathbf{x}_i$  with scalar per-trajectory confidence scores  $c_i^{(d)}$ ,  $d \in \{1, \dots, D_i\}$ . These provide an ordering of the plausibility of the various trajectories predicted for a given input. The scores must be non-negative and sum to 1 (i.e., form a valid probability distribution).

**Per-Prediction Request Uncertainty Score.** We also expect models to produce scalar uncertainty estimates corresponding to each prediction request input  $\mathbf{x}_i$ . For example, on evaluation dataset  $\mathcal{D}_{\text{eval}}^j$ , we have  $M_j$  per-prediction request uncertainty scores  $\{U_i \mid i \in 1, \dots, M_j\}$ . These correspond to the model’s uncertainty in making any trajectory prediction for the agent of interest. In a real-world deployment setting, a self-driving vehicle would associate a high per-prediction request uncertainty score with a scene context that is particularly unfamiliar or high-risk.

Next, we will describe standard motion prediction performance metrics, followed by confidence-aware metrics which reward models with well-calibrated uncertainty.

## 5.3 Metrics

**Standard Performance Metrics.** We assess the performance of a motion prediction system using several standard metrics.

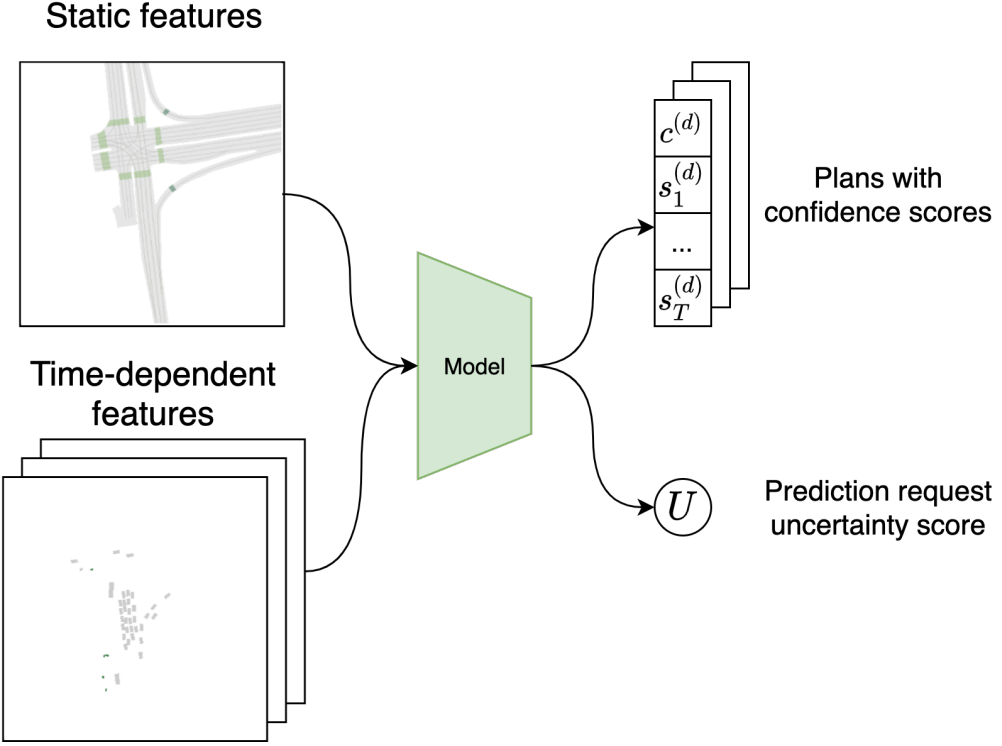


Figure 10: Diagram of the Vehicle Motion Prediction task. Models take as input a single scene context  $\mathbf{x}$  composed of static (HD map) and time-dependent input features, and predict trajectories  $\{\mathbf{y}^{(d)} \mid d \in 1, \dots, D\}$  with corresponding per-trajectory confidence scores  $\{c^{(d)} \mid d \in 1, \dots, D\}$ , as well as a single per-prediction request uncertainty score  $U$ .

The average displacement error (ADE) measures the quality of a predicted trajectory  $\mathbf{y}$  with respect to the ground truth trajectory  $\mathbf{y}^*$  as

$$\text{ADE}(\mathbf{y}) := \frac{1}{T} \sum_{t=1}^T \|s_t - s_t^*\|_2, \quad (4)$$

where  $\mathbf{y} = (s_1, \dots, s_T)$ . Analogously, the final displacement error

$$\text{FDE}(\mathbf{y}) := \|s_T - s_T^*\|_2, \quad (5)$$

measures the quality at the last timestep.

Stochastic models define a predictive distribution  $q(\mathbf{y} \mid \mathbf{x}; \theta)$ , and can therefore be evaluated over the  $D$  trajectories sampled for a given input  $\mathbf{x}$ . For example, we can measure an aggregated ADE over  $D$  samples with

$$\text{aggADE}_D(q) := \bigoplus_{\{\mathbf{y}\}_{d=1}^D \sim q(\mathbf{y} \mid \mathbf{x})} \text{ADE}(\mathbf{y}^d), \quad (6)$$

where  $\oplus$  is an aggregation operator, e.g.,  $\oplus = \min$  recovers the minimum ADE (minADE $_D$ ) commonly used in evaluation of stochastic motion prediction models [69, 63]. We consider minimum and mean aggregation of the average displacement error (minADE, avgADE), as well as of the final displacement error (minFDE, avgFDE).

**Per-Trajectory Confidence-Aware Metrics.** A stochastic model used in practice for motion prediction must ultimately *decide* on a particular predicted trajectory for a given prediction request. We may make this decision by selecting for evaluation the predicted trajectory with the highest per-trajectory confidence score. In other words, given per-trajectory confidence scores  $\{c^{(d)} \mid d \in 1, \dots, D\}$  we select the top trajectory  $y^{(d*)}$ ,  $d^* = \arg \max_d c^{(d)}$ , and measure the decision quality using *top1* ADE

and FDE metrics, e.g.,

$$\text{top1ADE}_D(q) := \text{ADE}(\mathbf{y}^{(d^*)}). \quad (7)$$

We may also wish to assess the quality of the relative weighting of the  $D$  trajectories with their corresponding per-trajectory confidence scores  $c^{(d)}$ . This is accomplished with a weighted metric

$$\text{weightedADE}_D(q) := \sum_{d \in D} c^{(d)} \cdot \text{ADE}(\mathbf{y}^{(d)}). \quad (8)$$

The top1FDE and weightedFDE metrics follow analogously to the above.

**Per-Prediction Request Confidence-Aware Metrics.** In addition to making a decision amongst many possible trajectories in a particular situation, a motion planning agent should know when, in general, any trajectories it predicts will be inaccurate (e.g., due to unfamiliarity of the setting, or inherent ambiguity in the path of the vehicle for which a prediction is requested). We evaluate the quality of uncertainty quantification jointly with robustness to distributional shift using the retention-based metrics described in Section 2, with the per-prediction request uncertainty scores determining retention order. Note that each retention curve is plotted with respect to a particular error metric above (e.g., we consider AUC for retention with respect to weightedADE). Additionally, we also assess whether the per-prediction uncertainty scores can be used to discriminate between in-domain and shifted scenes. In this case, quality is assessed via area under a ROC curve.

#### 5.4 Baselines Results

**Robust Imitative Planning.** As our baseline we consider Robust Imitative Planning (RIP) [69], where an ensemble of probabilistic models is used to stochastically generate multiple predictions for a given prediction request. We adapt the method to produce uncertainty estimates at our two desired levels of granularity: per-trajectory and per-prediction request. In detail, we use the following approach for trajectory and confidence score generation.

- 1) **Trajectory Generation.** Given a scene input  $x$ ,  $K$  ensemble members generate  $G$  trajectories.<sup>10</sup>
- 2) **Trajectory Scoring.** We score each of the  $G$  trajectories by computing a log probability under each of the  $K$  trained likelihood models.
- 3) **Per-Trajectory Confidence Scores.** We aggregate the  $G \cdot K$  resulting log probabilities to  $G$  scores using a per-trajectory aggregation operator  $\oplus_{\text{trajectory}}$ .<sup>11</sup> By aggregating over the log-likelihood estimates sampled from the model posterior (i.e., contributed by each ensemble member), we obtain a robust score for each of the  $G$  trajectories [69].
- 4) **Trajectory Selection.** Among the  $G$  trajectories, the RIP ensemble produces the top  $D$  trajectories as determined by their corresponding  $G$  per-trajectory confidence scores, where  $D$  is a hyperparameter.
- 5) **Per-Prediction Request Uncertainty Score.** We aggregate the  $D$  top per-trajectory confidence scores to a single uncertainty score  $U$  using the aggregator  $\oplus_{\text{pred-req}}$ .<sup>12</sup> This value conveys the ensemble’s estimated uncertainty for a given scene context and a particular prediction request.
- 6) **Confidence Reporting.** We obtain scores  $c^{(d)}$  by applying a softmax to the  $D$  top per-trajectory confidence scores. We report these  $c^{(d)}$  and  $U$  (computed in step 5) as our final per-trajectory confidence scores and per-prediction request uncertainty score, respectively.

To summarize, our implementation of RIP for motion prediction produces  $D$  trajectories and corresponding normalized per-trajectory scores  $\{c^{(d)} \mid d \in 1, \dots, D\}$ , as well as an aggregated uncertainty score  $U$  for the overall prediction request.

<sup>10</sup>In practice, each ensemble member generates the same number of trajectories  $Q$ , s.t.  $G = K \cdot Q$ .

<sup>11</sup>For example, applying a `min` aggregation is informed by robust control literature [71] in which we aim to optimize for the worst-case scenario, as measured by the log-likelihood of the “most pessimistic” model for a given trajectory.

<sup>12</sup>In practice, this is done by applying the aggregation (e.g.,  $\oplus_{\text{pred-req}} = \text{mean}$ ) to the confidences  $c^{(d)}$ , and then *negating* to obtain the uncertainty score  $U$ .

**Backbone Likelihood Model.** We consider two different model classes as ensemble members: a simple behavioral cloning agent with a Gated Recurrent Unit decoder (BC) [72, 73] and a Deep Imitative Model (DIM) [74] with an autoregressive flow decoder [75], following [69]. In both cases, we model the likelihood of a trajectory  $\mathbf{y}$  in context  $\mathbf{x}$  to come from an expert (i.e., from the distribution of ground truth trajectories), with learnable parameters  $\theta$ , as

$$q(\mathbf{y} \mid \mathbf{x}; \theta) = \prod_{t=1}^T p(s_t \mid \mathbf{y}_{<t}, \mathbf{x}; \theta) = \prod_{t=1}^T \mathcal{N}(s_t; \mu(\mathbf{y}_{<t}, \mathbf{x}; \theta), \Sigma(\mathbf{y}_{<t}, \mathbf{x}; \theta)), \quad (9)$$

where  $\mu(\cdot; \theta)$  and  $\Sigma(\cdot; \theta)$  are two heads of a recurrent neural network with shared torso. Hence we assume that the conditional densities are normally distributed, and learn those parameters through maximum likelihood estimation. Notably, for the BC model, we found that conditioning on samples  $\hat{\mathbf{y}}_{<t}$  instead of ground truth values  $\mathbf{y}_{<t}$  (where usage of ground truth is often referred to as teacher forcing in RNN literature) significantly improved performance across all datasets and metrics.

**Setup.** We report performance of RIP across the two backbone models – Behavioral Cloning (BC) [73] and Deep Imitative Model (DIM) [74] – on development (dev) and evaluation (eval) datasets in in-distribution (In), distributionally shifted (Shifted), and combined in-distribution and shifted (Full) settings. With both backbone model classes we vary the number of ensemble members  $K \in \{1, 3, 5\}$ , train with learning rate 1e-4, use a cosine annealing LR schedule with 1 epoch warmup, and use gradient clipping at 1. We sample  $Q = 10$  trajectories from each of the ensemble members. We consider two types of aggregation: “Lower Quartile” in which we compute the mean minus the standard deviation  $\mu - \sigma$  of the input scores, and “Model Averaging” (MA) in which we compute the mean  $\mu$  of the input scores. LQ reflects the intuition to assign a high score to a trajectory when the ensemble members assign it a high score on average, and tend to be certain (have a low standard deviation) in their scoring; MA reflects only the prior intuition. This aggregation strategy (LQ or MA) is used as both the per-trajectory aggregation operator  $\oplus_{\text{trajectory}}$  and the per-prediction request aggregation operator  $\oplus_{\text{pred-req}}$  (where the latter is followed by negation to obtain an uncertainty, as opposed to a confidence). We fix the RIP ensemble at all  $K$  to produce the top  $D = 5$  trajectories as ranked by their per-trajectory confidence score.

**Aggregate Results.** See Table 13 for the predictive performance of Robust Imitative Planning across the partitions of the dev and eval datasets, as measured by standard and per-trajectory confidence-aware metrics. We observe that RIP (BC) consistently outperforms RIP (DIM) on the per-trajectory confidence weighted metrics (weightedADE and weightedFDE), and RIP (DIM) outperforms RIP (BC) on minADE and minFDE. This result might occur if DIM has higher predictive variance. In such a case, DIM might be more effective in modeling multimodality, and therefore would tend to produce at least one high accuracy trajectory on more scenes, improving performance on min aggregation metrics. On the other hand, for “obvious” scenes, DIM might then produce unnecessarily complicated trajectories which would be reflected in poor performance on weighted aggregation metrics. Model Averaging (MA) outperforms Lower Quartile (LQ) aggregation, and ensembling improves performance across the metrics. Across all model configurations and these four predictive metrics, performance on the distributionally shifted dataset is worse than that on the in-distribution dataset.

See Table 14 for the uncertainty and robustness performance of Robust Imitative Planning. The R-AUC, F1-AUC, and F1@95% metrics are computed with respect to the weightedADE metric. Interestingly, we find that the performance on the distributionally shifted dev dataset exceeds that on the in-distribution dev dataset: for example, R-AUC for the 5-model BC ensemble with MA aggregation (BC, MA,  $K = 5$ ) on in-distribution dev achieves AUC = 0.242, versus AUC = 0.205 for shifted dev, where lower is better. One potential explanation is that there are certain examples on which the model performs particularly poorly in the shifted datasets, and that on retention tasks, their disproportionate contribution to the loss metric can be mitigated with well-calibrated uncertainty (a particularly high uncertainty on those examples). Additionally, we find that across model configurations and aggregation operators, the per-prediction request uncertainty scores do not perform particularly well in detecting distribution shift (ROC-AUC). This may occur due to significant data uncertainty in all cases. Future work on detecting distributional shift in the Vehicle Motion Prediction dataset could, for example, inspect the distribution of log-likelihood scores on the in-distribution and shifted partitions in order to devise a metric for this task, aside from the uncertainty scores  $U$  used for the retention analysis.

Table 13: *Predictive performance* of the two RIP variants – behavioral cloning (BC) [73] and Deep Imitative Model (DIM) [74] – on the development and evaluation datasets. Each section contains losses computed over the in-distribution (In), distributionally shifted (Shifted), and combined (Full) development and evaluation datasets. We vary the backbone model, aggregation strategy (applied for both the per-trajectory aggregation operator  $\oplus_{\text{trajectory}}$  and the per-prediction request aggregation operator  $\oplus_{\text{pred-req}}$ ), and the number of ensemble members  $K$ . The top performer for each metric and dataset split is **bolded**. See Section 5.4 for setup details.

Dataset	Model	minADE ↓			weightedADE ↓			minFDE ↓			weightedFDE ↓		
		In	Shifted	Full	In	Shifted	Full	In	Shifted	Full	In	Shifted	Full
Dev	BC, LQ, K=1	0.818	0.960	0.835	1.088	1.245	1.107	1.718	2.113	1.765	2.368	2.777	2.417
	BC, LQ, K=3	0.780	0.909	0.795	1.040	1.170	1.056	1.638	2.018	1.683	2.254	2.609	2.297
	BC, LQ, K=5	0.766	0.888	0.780	1.017	1.138	1.031	1.618	1.980	1.661	2.214	2.552	2.254
	BC, MA, K=1	0.818	0.960	0.835	1.088	1.245	1.107	1.718	2.113	1.765	2.368	2.777	2.417
	BC, MA, K=3	0.780	0.908	0.795	1.034	1.166	1.050	1.641	2.018	1.686	2.249	2.611	2.292
	BC, MA, K=5	0.765	0.887	0.779	<b>1.012</b>	<b>1.133</b>	<b>1.026</b>	1.617	1.976	1.660	<b>2.210</b>	<b>2.551</b>	<b>2.251</b>
	DIM, LQ, K=1	0.750	0.818	0.758	1.523	1.583	1.530	1.497	1.720	1.524	3.472	3.639	3.492
	DIM, LQ, K=3	<b>0.717</b>	0.787	<b>0.725</b>	1.407	1.470	1.415	1.467	1.687	1.493	3.219	3.397	3.240
	DIM, LQ, K=5	0.720	0.787	0.728	1.399	1.470	1.407	1.487	1.704	1.513	3.202	3.397	3.225
	DIM, MA, K=1	0.750	0.818	0.758	1.523	1.583	1.530	1.497	1.720	1.524	3.472	3.639	3.492
Eval	DIM, MA, K=3	<b>0.717</b>	<b>0.785</b>	<b>0.725</b>	1.410	1.475	1.418	<b>1.466</b>	<b>1.685</b>	<b>1.492</b>	3.226	3.409	3.248
	DIM, MA, K=5	0.719	0.786	0.727	1.399	1.469	1.408	1.482	1.698	1.508	3.202	3.393	3.225
	BC, LQ, K=1	0.829	1.084	0.880	1.104	1.407	1.164	1.733	2.420	1.870	2.394	3.197	2.555
	BC, LQ, K=3	0.792	1.026	0.839	1.056	1.326	1.110	1.658	2.297	1.786	2.284	3.005	2.429
	BC, LQ, K=5	0.777	1.015	0.825	1.032	1.303	1.086	1.636	2.283	1.765	2.242	2.964	2.386
	BC, MA, K=1	0.829	1.084	0.880	1.104	1.407	1.164	1.733	2.420	1.870	2.394	3.197	2.555
	BC, MA, K=3	0.792	1.025	0.838	1.050	1.319	1.104	1.661	2.294	1.788	2.278	2.997	2.422
	BC, MA, K=5	0.777	1.014	0.824	<b>1.028</b>	<b>1.299</b>	<b>1.082</b>	1.636	2.278	1.765	<b>2.238</b>	<b>2.957</b>	<b>2.382</b>
	DIM, LQ, K=1	0.759	0.942	0.796	1.551	1.883	1.618	1.511	1.983	1.605	3.536	4.376	3.704
	DIM, LQ, K=3	<b>0.726</b>	0.914	0.764	1.433	1.756	1.498	1.481	1.972	1.579	3.277	4.094	3.440
Eval	DIM, LQ, K=5	0.729	0.921	0.768	1.422	1.757	1.489	1.498	2.007	1.600	3.253	4.098	3.422
	DIM, MA, K=1	0.759	0.942	0.796	1.551	1.883	1.618	1.511	1.983	1.605	3.536	4.376	3.704
	DIM, MA, K=3	<b>0.726</b>	<b>0.912</b>	<b>0.763</b>	1.437	1.759	1.502	<b>1.478</b>	<b>1.967</b>	<b>1.576</b>	3.286	4.101	3.449
	DIM, MA, K=5	0.728	0.918	0.766	1.424	1.754	1.490	1.493	2.000	1.595	3.256	4.093	3.424

Table 14: *Uncertainty and robustness performance* of the two RIP variants. The top performer for each metric and dataset split is **bolded**. The error metric for computing the area under the rejection curve (R-AUC) and area under the F1 curve (F1-AUC) is **weightedADE**. See Section 5.4 for setup details.

Dataset	Model	R-AUC ↓			F1-AUC ↑			F1@95% ↑			ROC-AUC (%) ↑		
		In	Shifted	Full	In	Shifted	Full	In	Shifted	Full	In	Shifted	Full
Dev	BC, LQ, K=1	0.272	0.244	0.268	0.670	<b>0.685</b>	0.672	0.836	0.866	0.840	51.0		
	BC, LQ, K=3	0.316	0.249	0.307	0.643	0.676	0.648	0.815	0.864	0.821	46.7		
	BC, LQ, K=5	0.275	0.220	0.266	0.659	0.682	0.662	0.837	0.875	0.842	47.3		
	BC, MA, K=1	0.272	0.244	0.268	0.670	<b>0.685</b>	0.672	0.836	0.866	0.840	51.0		
	BC, MA, K=3	0.258	0.219	0.252	0.669	0.684	0.672	0.845	0.877	0.849	48.6		
	BC, MA, K=5	<b>0.242</b>	<b>0.205</b>	<b>0.236</b>	<b>0.672</b>	0.684	<b>0.674</b>	<b>0.850</b>	<b>0.879</b>	<b>0.854</b>	49.2		
	DIM, LQ, K=1	0.431	0.364	0.423	0.623	0.651	0.627	0.792	0.860	0.800	<b>51.8</b>		
	DIM, LQ, K=3	0.387	0.328	0.380	0.633	0.655	0.635	0.802	0.864	0.809	51.4		
	DIM, LQ, K=5	0.382	0.324	0.376	0.635	0.656	0.638	0.802	0.865	0.810	51.4		
	DIM, MA, K=1	0.427	0.360	0.419	0.627	0.653	0.630	0.792	0.860	0.801	<b>51.8</b>		
Eval	DIM, MA, K=3	0.388	0.328	0.381	0.634	0.656	0.637	0.801	0.863	0.809	51.4		
	DIM, MA, K=5	0.383	0.324	0.376	0.636	0.657	0.639	0.802	0.865	0.809	51.4		
	BC, LQ, K=1	0.279	0.356	0.293	0.669	0.675	0.671	0.832	0.793	0.824	<b>52.8</b>		
	BC, LQ, K=3	0.321	0.353	0.327	0.643	0.663	0.647	0.811	0.792	0.808	50.9		
	BC, LQ, K=5	0.280	0.320	0.287	0.659	0.673	0.662	0.833	0.808	0.828	51.4		
	BC, MA, K=1	0.279	0.356	0.293	0.670	0.675	0.671	0.832	0.793	0.824	<b>52.8</b>		
	BC, MA, K=3	0.264	0.320	0.274	0.669	0.678	0.671	0.841	0.809	0.835	51.3		
	BC, MA, K=5	<b>0.247</b>	<b>0.305</b>	<b>0.258</b>	<b>0.673</b>	<b>0.679</b>	<b>0.674</b>	<b>0.846</b>	<b>0.814</b>	<b>0.840</b>	52.1		
	DIM, LQ, K=1	0.446	0.530	0.462	0.621	0.628	0.622	0.786	0.767	0.782	52.0		
	DIM, LQ, K=3	0.401	0.483	0.416	0.631	0.637	0.632	0.796	0.776	0.792	51.4		
Eval	DIM, LQ, K=5	0.394	0.479	0.410	0.633	0.640	0.635	0.797	0.777	0.793	51.2		
	DIM, MA, K=1	0.442	0.526	0.458	0.624	0.632	0.626	0.786	0.767	0.783	51.8		
	DIM, MA, K=3	0.401	0.484	0.417	0.632	0.639	0.633	0.795	0.776	0.791	51.1		
	DIM, MA, K=5	0.395	0.479	0.411	0.634	0.641	0.636	0.797	0.777	0.793	50.9		

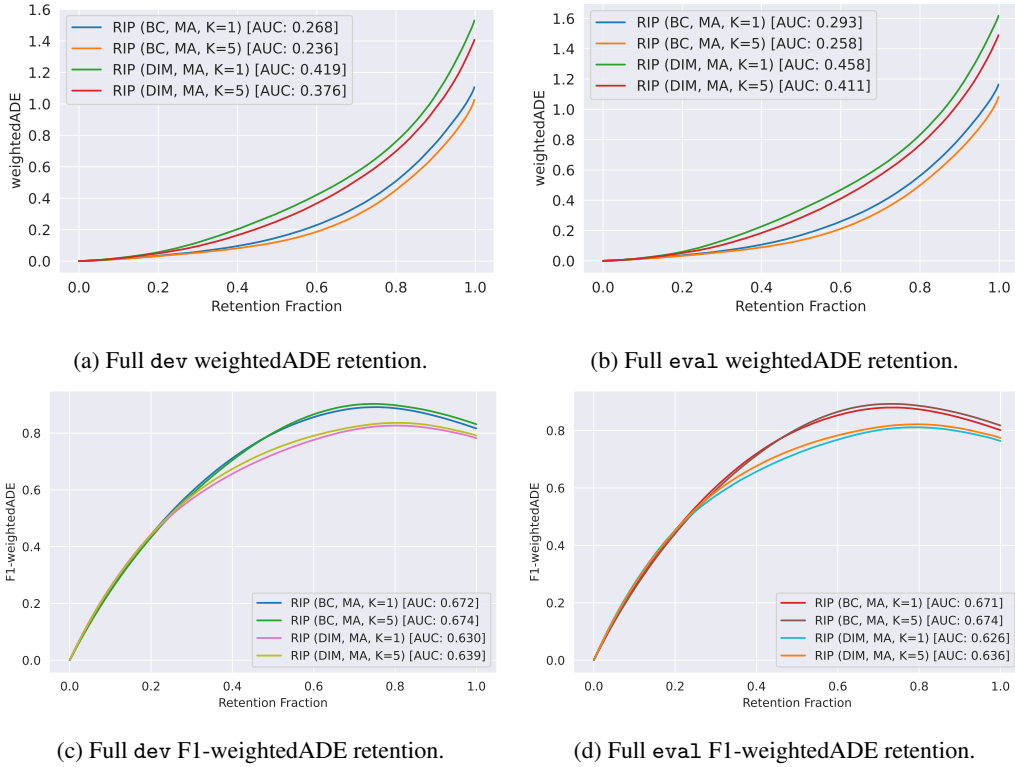


Figure 11: weightedADE and F1-weightedADE retention curves on the Full (i.e., containing both the in-distribution and distributionally shifted datapoints) dev (left column) and eval (right column) partitions of the Vehicle Motion Prediction dataset. Top row: retention on weightedADE (lower  $\downarrow$  AUC is better). Bottom row: retention on F1-weightedADE (higher  $\uparrow$  AUC is better). We vary the backbone model and number of ensemble members, fix the Model Averaging (MA) aggregation strategy for the per-trajectory aggregation operator  $\oplus_{\text{trajectory}}$  and the per-prediction request aggregation operator  $\oplus_{\text{pred-req}}$  (based on results from Table 14), and otherwise use the standard RIP settings enumerated in Section 5.4.

**Retention Results.** See Fig. 11 for retention on weightedADE (top row) and F1-weightedADE (bottom row) on the Full dev and eval partitions. Based on the results from Table 14 we display only the Model Averaging (MA) aggregation, and vary between BC and DIM as well as  $K \in \{1, 5\}$ . Across all retention tasks, RIP (BC, MA,  $K = 5$ ) achieves the best AUC. For both backbone models and the Model Averaging aggregation, ensembling improves AUC.

## 6 Conclusion

In this paper, we proposed the **Shifts Dataset**: a large, standardized dataset for evaluation of uncertainty estimates and robustness to realistic, curated distributional shift. The dataset – sourced from industrial services – is composed of three tasks, with each corresponding to a particular data modality: *tabular weather prediction*, *machine translation*, and *self-driving car (SDC) vehicle motion prediction*. In this work, we describe this data and provide baseline results using ensemble methods. Given the current state of the field, where most methods are developed on small-scale classification tasks, we aim to draw the attention of the community to the evaluation of uncertainty estimation and robustness to distributional shift on a large, realistic, and standardized set of large-scale tasks across a range of modalities. We believe this work is a necessary step towards meaningful evaluation of the plethora of uncertainty quantification methods, and hope for it to accelerate the development of this area and safe ML in general.

## Acknowledgments and Disclosure of Funding

We would like to thank Yandex for providing the data and resources necessary in benchmark creation. We thank Intel and the Turing Institute for funding the work of the OATML Group on this project.

## References

- [1] Karen Simonyan and Andrew Zisserman, “Very Deep Convolutional Networks for Large-Scale Image Recognition,” in *Proc. International Conference on Learning Representations (ICLR)*, 2015.
- [2] Tomas Mikolov et al., “Linguistic Regularities in Continuous Space Word Representations,” in *Proc. NAACL-HLT*, 2013.
- [3] Tomas Mikolov, Martin Karafiat, Lukas Burget, Jan Cernocky, and Sanjeev Khudanpur, “Recurrent Neural Network Based Language Model,” in *Proc. INTERSPEECH*, 2010.
- [4] Dzmitry Bahdanau, Kyunghyun Cho, and Yoshua Bengio, “Neural machine translation by jointly learning to align and translate,” in *Proc. International Conference on Learning Representations (ICLR)*, 2015.
- [5] Ashish Vaswani, Noam Shazeer, Niki Parmar, Jakob Uszkoreit, Llion Jones, Aidan N Gomez, Łukasz Kaiser, and Illia Polosukhin, “Attention is all you need,” in *Advances in neural information processing systems*, 2017, pp. 5998–6008.
- [6] Geoffrey Hinton, Li Deng, Dong Yu, George Dahl, Abdel Rahman Mohamed, Navdeep Jaitly, Andrew Senior, Vincent Vanhoucke, Patrick Nguyen, Tara Sainath, and Brian Kingsbury, “Deep neural networks for acoustic modeling in speech recognition,” *Signal Processing Magazine*, 2012.
- [7] Joaquin Quiñonero-Candela, *Dataset Shift in Machine Learning*, The MIT Press, 2009.
- [8] Pang Wei Koh, Shiori Sagawa, Henrik Marklund, Sang Michael Xie, Marvin Zhang, Akshay Balsubramani, Weihua Hu, Michihiro Yasunaga, Richard Lanas Phillips, Sara Beery, Jure Leskovec, Anshul Kundaje, Emma Pierson, Sergey Levine, Chelsea Finn, and Percy Liang, “Wilds: A benchmark of in-the-wild distribution shifts,” 2020.
- [9] Dario Amodei, Chris Olah, Jacob Steinhardt, Paul F. Christiano, John Schulman, and Dan Mané, “Concrete problems in AI safety,” <http://arxiv.org/abs/1606.06565>, 2016, arXiv: 1606.06565.
- [10] Yarin Gal, *Uncertainty in Deep Learning*, Ph.D. thesis, University of Cambridge, 2016.
- [11] Andrey Malinin, *Uncertainty Estimation in Deep Learning with application to Spoken Language Assessment*, Ph.D. thesis, University of Cambridge, 2019.
- [12] Yarin Gal and Zoubin Ghahramani, “Dropout as a Bayesian Approximation: Representing Model Uncertainty in Deep Learning,” in *Proc. 33rd International Conference on Machine Learning (ICML-16)*, 2016.
- [13] B. Lakshminarayanan, A. Pritzel, and C. Blundell, “Simple and Scalable Predictive Uncertainty Estimation using Deep Ensembles,” in *Proc. Conference on Neural Information Processing Systems (NIPS)*, 2017.
- [14] Arsenii Ashukha, Alexander Lyzhov, Dmitry Molchanov, and Dmitry Vetrov, “Pitfalls of in-domain uncertainty estimation and ensembling in deep learning,” in *International Conference on Learning Representations*, 2020.
- [15] Yaniv Ovadia, Emily Fertig, Jie Ren, Zachary Nado, D Sculley, Sebastian Nowozin, Joshua V Dillon, Balaji Lakshminarayanan, and Jasper Snoek, “Can you trust your model’s uncertainty? evaluating predictive uncertainty under dataset shift,” *Advances in Neural Information Processing Systems*, 2019.
- [16] Nicholas Carlini and David A. Wagner, “Adversarial examples are not easily detected: Bypassing ten detection methods,” *CoRR*, 2017.
- [17] L. Smith and Y. Gal, “Understanding Measures of Uncertainty for Adversarial Example Detection,” in *UAI*, 2018.

- [18] Andreas Kirsch, Joost Van Amersfoort, and Yarin Gal, “Batchbald: Efficient and diverse batch acquisition for deep bayesian active learning,” *Advances in neural information processing systems*, vol. 32, pp. 7026–7037, 2019.
- [19] Tim Z Xiao, Aidan N Gomez, and Yarin Gal, “Wat heb je gezegd? detecting out-of-distribution translations with variational transformers,” in *Bayesian Deep Learning Workshop (NeurIPS)*, 2019.
- [20] Pascal Notin, José Miguel Hernández-Lobato, and Yarin Gal, “Principled uncertainty estimation for high dimensional data,” in *Uncertainty & Robustness in Deep Learning Workshop, ICML*, 2020.
- [21] Marina Fomicheva, Shuo Sun, Lisa Yankovskaya, Frédéric Blain, Francisco Guzmán, Mark Fishel, Nikolaos Aletras, Vishrav Chaudhary, and Lucia Specia, “Unsupervised quality estimation for neural machine translation,” *arXiv preprint arXiv:2005.10608*, 2020.
- [22] Tim Z Xiao, Aidan N Gomez, and Yarin Gal, “Wat heb je gezegd? detecting out-of-distribution translations with variational transformers,” 2019.
- [23] Andrey Malinin and Mark Gales, “Uncertainty estimation in autoregressive structured prediction,” in *International Conference on Learning Representations*, 2021.
- [24] Shiyu Liang, Yixuan Li, and R. Srikanth, “Enhancing the reliability of out-of-distribution image detection in neural networks,” 2020.
- [25] Yen-Chang Hsu, Yilin Shen, Hongxia Jin, and Zsolt Kira, “Generalized odin: Detecting out-of-distribution image without learning from out-of-distribution data,” 2020.
- [26] Joost Van Amersfoort, Lewis Smith, Yee Whye Teh, and Yarin Gal, “Uncertainty estimation using a single deep deterministic neural network,” in *International Conference on Machine Learning*. PMLR, 2020, pp. 9690–9700.
- [27] Marton Havasi, Rodolphe Jenatton, Stanislav Fort, Jeremiah Zhe Liu, Jasper Snoek, Balaji Lakshminarayanan, Andrew M. Dai, and Dustin Tran, “Training independent subnetworks for robust prediction,” 2020.
- [28] Jeremiah Zhe Liu, Zi Lin, Shreyas Padhy, Dustin Tran, Tania Bedrax-Weiss, and Balaji Lakshminarayanan, “Simple and principled uncertainty estimation with deterministic deep learning via distance awareness,” *arXiv preprint arXiv:2006.10108*, 2020.
- [29] Joost van Amersfoort, Lewis Smith, Andrew Jesson, Oscar Key, and Yarin Gal, “Improving deterministic uncertainty estimation in deep learning for classification and regression,” *arXiv preprint arXiv:2102.11409*, 2021.
- [30] Jishnu Mukhoti, Andreas Kirsch, Joost van Amersfoort, Philip HS Torr, and Yarin Gal, “Deterministic neural networks with appropriate inductive biases capture epistemic and aleatoric uncertainty,” *arXiv preprint arXiv:2102.11582*, 2021.
- [31] Andrey Malinin and Mark Gales, “Predictive uncertainty estimation via prior networks,” in *Advances in Neural Information Processing Systems*, 2018, pp. 7047–7058.
- [32] Andrey Malinin and Mark JF Gales, “Reverse kl-divergence training of prior networks: Improved uncertainty and adversarial robustness,” 2019.
- [33] Andrey Malinin, Sergey Chervontsev, Ivan Prosvilov, and Mark Gales, “Regression prior networks,” 2020.
- [34] Andrey Malinin, Bruno Mlodzeniec, and Mark JF Gales, “Ensemble distribution distillation,” in *International Conference on Learning Representations*, 2020.
- [35] Max Ryabinin, Andrey Malinin, and Mark Gales, “Scaling ensemble distribution distillation to many classes with proxy targets,” *arXiv preprint arXiv:2105.06987*, 2021.
- [36] Angelos Filos, Sebastian Farquhar, Aidan N. Gomez, Tim G. J. Rudner, Zachary Kenton, Lewis Smith, Milad Alizadeh, Arnoud de Kroon, and Yarin Gal, “A systematic comparison of bayesian deep learning robustness in diabetic retinopathy tasks,” 2019.
- [37] Dan Hendrycks, Steven Basart, Norman Mu, Saurav Kadavath, Frank Wang, Evan Dorundo, Rahul Desai, Tyler Zhu, Samyak Parajuli, Mike Guo, Dawn Song, Jacob Steinhardt, and Justin Gilmer, “The many faces of robustness: A critical analysis of out-of-distribution generalization,” 2020.

[38] Dan Hendrycks and Thomas Dietterich, “Benchmarking neural network robustness to common corruptions and perturbations,” 2019.

[39] Dan Hendrycks, Kevin Zhao, Steven Basart, Jacob Steinhardt, and Dawn Song, “Natural adversarial examples,” 2021.

[40] J. Deng, W. Dong, R. Socher, L.-J. Li, K. Li, and L. Fei-Fei, “ImageNet: A Large-Scale Hierarchical Image Database,” in *CVPR09*, 2009.

[41] Paul Michel and Graham Neubig, “MTNT: A testbed for Machine Translation of Noisy Text,” in *Proceedings of the 2018 Conference on Empirical Methods in Natural Language Processing (EMNLP)*, 2018.

[42] Y. LeCun, L. Bottou, Y. Bengio, and P. Haffner, “Gradient-based learning applied to document recognition,” *Proceedings of the IEEE*, vol. 86, pp. 2278–2324, 1998.

[43] Brenden M. Lake, Ruslan Salakhutdinov, and Joshua B. Tenenbaum, “Human-level concept learning through probabilistic program induction,” *Science*, vol. 350, no. 6266, pp. 1332–1338, 2015.

[44] Ian J. Goodfellow, Yaroslav Bulatov, Julian Ibarz, Sacha Arnoud, and Vinay D. Shet, “Multi-digit number recognition from street view imagery using deep convolutional neural networks,” 2013, arXiv:1312.6082.

[45] Alex Krizhevsky, “Learning multiple layers of features from tiny images,” 2009.

[46] Deliang Chen and Hans Weiteng Chen, “Using the köppen classification to quantify climate variation and change: An example for 1901–2010,” *Environmental Development*, vol. 6, pp. 69–79, 2013.

[47] Liudmila Prokhorenkova, Gleb Gusev, Aleksandr Vorobev, Anna Veronika Dorogush, and Andrey Gulin, “Catboost: unbiased boosting with categorical features,” in *Proceedings of the 32nd International Conference on Neural Information Processing Systems (NeurIPS)*, 2018, pp. 6638–6648.

[48] Andrey Malinin, Liudmila Prokhorenkova, and Aleksei Ustimenko, “Uncertainty in gradient boosting via ensembles,” in *International Conference on Learning Representations*, 2021.

[49] Shuo Wang, Yang Liu, Chao Wang, Huanbo Luan, and Maosong Sun, “Improving back-translation with uncertainty-based confidence estimation,” *arXiv preprint arXiv:1909.00157*, 2019.

[50] GlobalVoices, “Globalvoices,” <https://globalvoices.org/>.

[51] Matt Post, “A call for clarity in reporting BLEU scores,” in *Proceedings of the Third Conference on Machine Translation: Research Papers*, Belgium, Brussels, Oct. 2018, pp. 186–191, Association for Computational Linguistics.

[52] Courtney Napoles, Keisuke Sakaguchi, Matt Post, and Joel Tetreault, “Ground truth for grammatical error correction metrics,” in *Proceedings of the 53rd Annual Meeting of the Association for Computational Linguistics and the 7th International Joint Conference on Natural Language Processing (Volume 2: Short Papers)*, Beijing, China, July 2015, pp. 588–593, Association for Computational Linguistics.

[53] Courtney Napoles, Keisuke Sakaguchi, Matt Post, and Joel Tetreault, “GLEU without tuning,” *eprint arXiv:1605.02592 [cs.CL]*, 2016.

[54] Yonghui Wu, Mike Schuster, Zhifeng Chen, Quoc V Le, Mohammad Norouzi, Wolfgang Macherey, Maxim Krikun, Yuan Cao, Qin Gao, Klaus Macherey, et al., “Google’s neural machine translation system: Bridging the gap between human and machine translation,” *arXiv preprint arXiv:1609.08144*, 2016.

[55] Myle Ott, Sergey Edunov, Alexei Baevski, Angela Fan, Sam Gross, Nathan Ng, David Grangier, and Michael Auli, “fairseq: A fast, extensible toolkit for sequence modeling,” in *Proceedings of NAACL-HLT 2019: Demonstrations*, 2019.

[56] Rhiannon Michelmore, Marta Kwiatkowska, and Yarin Gal, “Evaluating uncertainty quantification in end-to-end autonomous driving control,” *arXiv preprint arXiv:1811.06817*, 2018.

[57] Alexandre Alahi, Kratarth Goel, Vignesh Ramanathan, Alexandre Robicquet, Li Fei-Fei, and Silvio Savarese, “Social lstm: Human trajectory prediction in crowded spaces,” in *Proceedings of the IEEE conference on computer vision and pattern recognition*, 2016, pp. 961–971.

[58] Namhoon Lee, Wongun Choi, Paul Vernaza, Christopher B Choy, Philip HS Torr, and Manmohan Chandraker, “Desire: Distant future prediction in dynamic scenes with interacting agents,” in *Proceedings of the IEEE Conference on Computer Vision and Pattern Recognition*, 2017, pp. 336–345.

[59] Agrim Gupta, Justin Johnson, Li Fei-Fei, Silvio Savarese, and Alexandre Alahi, “Social gan: Socially acceptable trajectories with generative adversarial networks,” in *Proceedings of the IEEE Conference on Computer Vision and Pattern Recognition*, 2018, pp. 2255–2264.

[60] Yuning Chai, Benjamin Sapp, Mayank Bansal, and Dragomir Anguelov, “Multipath: Multiple probabilistic anchor trajectory hypotheses for behavior prediction,” *arXiv preprint arXiv:1910.05449*, 2019.

[61] Sergio Casas, Cole Gulino, Renjie Liao, and Raquel Urtasun, “Spatially-aware graph neural networks for relational behavior forecasting from sensor data,” *arXiv preprint arXiv:1910.08233*, 2019.

[62] Henggang Cui, Vladan Radosavljevic, Fang-Chieh Chou, Tsung-Han Lin, Thi Nguyen, Tzu-Kuo Huang, Jeff Schneider, and Nemanja Djuric, “Multimodal trajectory predictions for autonomous driving using deep convolutional networks,” in *2019 International Conference on Robotics and Automation (ICRA)*. IEEE, 2019, pp. 2090–2096.

[63] Tung Phan-Minh, Elena Corina Grigore, Freddy A Boulton, Oscar Beijbom, and Eric M Wolff, “Covernet: Multimodal behavior prediction using trajectory sets,” in *Proceedings of the IEEE/CVF Conference on Computer Vision and Pattern Recognition*, 2020, pp. 14074–14083.

[64] Jiyang Gao, Chen Sun, Hang Zhao, Yi Shen, Dragomir Anguelov, Congcong Li, and Cordelia Schmid, “Vectornet: Encoding hd maps and agent dynamics from vectorized representation,” in *Proceedings of the IEEE/CVF Conference on Computer Vision and Pattern Recognition*, 2020, pp. 11525–11533.

[65] Yuriy Bikitairov, Maxim Stebelev, Irina Rudenko, Oleh Shliazhko, and Boris Yangel, “Prank: motion prediction based on ranking,” in *Advances in Neural Information Processing Systems*, H. Larochelle, M. Ranzato, R. Hadsell, M. F. Balcan, and H. Lin, Eds. 2020, vol. 33, pp. 2553–2563, Curran Associates, Inc.

[66] Sergio Casas, Cole Gulino, Simon Suo, Katie Luo, Renjie Liao, and Raquel Urtasun, “Implicit latent variable model for scene-consistent motion forecasting,” in *Computer Vision–ECCV 2020: 16th European Conference, Glasgow, UK, August 23–28, 2020, Proceedings, Part XXIII 16*. Springer, 2020, pp. 624–641.

[67] Ming Liang, Bin Yang, Rui Hu, Yun Chen, Renjie Liao, Song Feng, and Raquel Urtasun, “Learning lane graph representations for motion forecasting,” in *European Conference on Computer Vision*. Springer, 2020, pp. 541–556.

[68] Yicheng Liu, Jinghuai Zhang, Liangji Fang, Qinhong Jiang, and Bolei Zhou, “Multimodal motion prediction with stacked transformers,” in *Proceedings of the IEEE/CVF Conference on Computer Vision and Pattern Recognition*, 2021, pp. 7577–7586.

[69] Angelos Filos, Panagiotis Tsigkas, Rowan McAllister, Nicholas Rhinehart, Sergey Levine, and Yarin Gal, “Can autonomous vehicles identify, recover from, and adapt to distribution shifts?,” in *International Conference on Machine Learning*. PMLR, 2020, pp. 3145–3153.

[70] Kaiming He, Xiangyu Zhang, Shaoqing Ren, and Jian Sun, “Deep residual learning for image recognition,” in *Proceedings of the IEEE conference on computer vision and pattern recognition*, 2016, pp. 770–778.

[71] Abraham Wald, “Contributions to the Theory of Statistical Estimation and Testing Hypotheses,” *The Annals of Mathematical Statistics*, vol. 10, no. 4, pp. 299 – 326, 1939.

[72] Kyunghyun Cho, Bart Van Merriënboer, Caglar Gulcehre, Dzmitry Bahdanau, Fethi Bougares, Holger Schwenk, and Yoshua Bengio, “Learning phrase representations using rnn encoder–decoder for statistical machine translation,” *arXiv preprint arXiv:1406.1078*, 2014.

[73] Felipe Codevilla, Matthias Müller, Antonio López, Vladlen Koltun, and Alexey Dosovitskiy, “End-to-end driving via conditional imitation learning,” in *2018 IEEE International Conference on Robotics and Automation (ICRA)*. IEEE, 2018, pp. 4693–4700.

[74] Nicholas Rhinehart, Rowan McAllister, and Sergey Levine, “Deep imitative models for flexible inference, planning, and control,” *CoRR*, vol. abs/1810.06544, 2018.

[75] Danilo Jimenez Rezende and Shakir Mohamed, “Variational inference with normalizing flows,” 2016.